

Melonic Dominance in Subchromatic Sextic Tensor Models

Shiroman Prakash^a and Ritam Sinha^b

^a *Department of Physics and Computer Science, Dayalbagh Educational Institute, Agra
282005, India*

^b *Instituto de Fisica Teorica IFT-UAM/CSIC, Cantoblanco 28049, Madrid. Spain*

Abstract

We study tensor models based on $O(N)^r$ symmetry groups constructed out of rank- r tensors with order- q interaction vertices. We define *subchromatic* tensor models to be those for which $r < q - 1$. We focus most of our attention on sextic ($q = 6$) models with maximally-single-trace interactions. We show that only a handful of subchromatic sextic maximally-single-trace interaction vertices exist. For each interaction we demonstrate that the set of Feynman diagrams that contribute to the free energy in the large N limit are melonic (or closely related to melonic diagrams) and thus can be explicitly summed.

Contents

1	Introduction and summary	2
2	Preliminaries	4
3	Sextic maximally-single-trace interactions	7
3.1	Constructing all sextic maximally-single-trace interactions	7
3.2	Automorphism and colour permutation symmetry	10
4	Large N limit of sub-chromatic maximally-single-trace interactions	12
4.1	Large N scaling of coupling constants	12
4.2	Existence of a loop passing through one or two vertices	14
5	Melonic dominance of subchromatic interaction vertices	15
5.1	Wheel	19
5.1.1	1-cycles	20
5.1.2	2-cycles	20
5.2	$r = 4$ Double-prism	22
5.2.1	1-cycles	23
5.2.2	2-cycles	23
5.3	$r = 3$ Prism	25
5.3.1	1-cycles	26
5.3.2	2-cycles	26
5.3.3	New cutting and sewing argument	28
5.4	Theory with both a prism and wheel	30
6	Comments on field-theories based on these interactions	30
6.1	Real sextic bosonic theories with melonic dominance	31
7	Discussion	32
A	Appendix: Finding inequivalent 2-cycles	33

1 Introduction and summary

In addition to well-known adjoint/matrix model [1] and vector model large N limits [2], a new large N limit dominated by melonic diagrams has attracted a great deal of attention recently [3–11]. The melonic limit was first observed in tensor models (see [12–15] for reviews), but interest in this limit grew due in large part to its appearance in the SYK model [16–18] which serves as a very educational toy model for quantum gravity [19–38].

Here we seek better understand the entire range of models for which melonic diagrams dominate. While there are important dynamical differences between the SYK model and tensor models [39, 40], tensor models provide a very natural context for understanding the diagrammatics of the melonic large N limit, and its possible generalizations.

Motivated by [41–44], we consider the large N limit of tensor models constructed out of rank- r tensors which transform in a representation of $O(N)^r$, with order- q , i.e., ϕ^q , interactions [14]. Each index transforms in the fundamental representation of its corresponding $O(N)$ symmetry group. Because r determines the number of colours used in a multi-line ‘t Hooft notation, we may also refer to r as the number of “colours” of the model. We refer to models with $r < q - 1$ as *sub-chromatic*.

It is natural to restrict our attention to interaction vertices that are *maximally-single-trace* (MST) [41, 44]. (We review the definition of maximally-single-trace, and other basic features of these theories in section 2.) In the large N limit, we expect that the maximally-single-trace interactions are the “most interesting” interactions, in the same sense that the tetrahedron is more interesting than the pillow and double-trace interactions for $q = 4$ theories.¹ We also remark that the restriction to maximally-single-trace operators reduces the number of interactions to a much more manageable number.

Let us discuss the large N limit of theories based on such interactions. When $r = 2$, these theories define the familiar “bifundamental” model [45, 46], in the large N limit, in which all planar diagrams survive. When $r = q - 1$, these theories are dominated by melonic diagrams, as recently argued in [44]. For interaction vertices with intermediate values of r , i.e., $2 < r < q - 1$, we can attempt to determine the set of diagrams which survive in the natural large N limit on a case-by-case basis – these will certainly include melonic diagrams, but additional diagrams may also contribute. An example of this is the prismatic² limit of [43], where additional diagrams contribute compared to the $r = 5$ sextic tensor model [44], such as the one shown in Figure 1.

In this paper, we focus our attention on the case of $q = 6$ with $O(N)$ interactions. This case is the smallest non-trivial case to consider. This case is also interesting because, in addition to studying quantum mechanical models in one dimension, one can hope to define

¹To provide some justification for this expectation, we observe that all the sextic non-MST interactions in [43] can be obtained from quartic pillow and double-trace interactions via an auxiliary field.

²The prismatic limit is solved by introducing an auxiliary field to rewrite the theory as a quartic tensor model with the familiar tetrahedron interaction. So one can argue that it is effectively still melonic. This limit can also be realized in a theory with random couplings, discussed in [47].

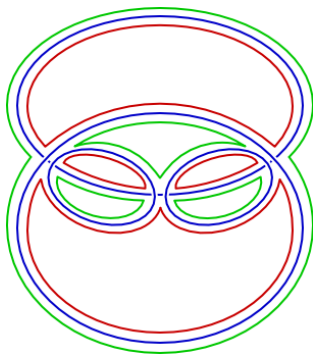


Figure 1: A maximal Feynman diagram in a theory with prism interactions that is not a conventionally melonic Feynman diagram. The diagram is proportional to $g^3 N^{12} = \lambda^3 N^3$.

quantum field theories with ϕ^6 interactions in $d \leq 3$ dimensions.

While one might be concerned that a large number of sub-chromatic vertices exist for generic q , the set of maximally-single-trace sub-chromatic vertices for $q = 6$ turns out to be very small, as we show in section 3. For $r = 3$, there are two interaction vertices – namely the prism and the wheel defined in [43] – and for $r = 4$, there is exactly one such interaction vertex, which we call the double-prism. In section 3 we also discuss the discrete symmetries of these interactions.

In section 4 we then discuss basic features of the large N limit of such theories: including the natural 't Hooft coupling and the existence of loops passing through one or two vertices. These results apply to all subchromatic maximally-single-trace interactions.

In section 5, we use the results of section 4 to characterize the set of free energy diagrams which survive in the large N limit for theories based on each of the three subchromatic maximally-single-trace interactions we identified in section 3. We also consider theories based on rank-3 tensors that contain both prism and wheel interactions. In all cases we find the diagrams can be explicitly summed, and these theories are effectively melonic – although, the case of the prism [43] might not be considered melonic in the conventional sense.

Let us point out³ that related work on sextic $U(N)^3$ and $U(N)^4$ theories appear in [48], where the melonic dominance of the wheel, also known as a $K_{3,3}$ interaction, is discussed following [49]. We believe our work is complementary to that of [48], as we consider $O(N)^r$ models, which allow for a larger number of maximally-single-trace interactions. In particular, we prove melonic dominance in the $r = 4$ theory based on the double-prism and the $r = 3$ theory involving both a prism and wheel interaction. Our arguments for melonic dominance are also self-contained and would hopefully be characterized as elementary.

In section 6 we briefly discuss the implications for bosonic and fermionic conformal field theories based on these interactions.

In section 7, we present conclusions and several avenues for future work.

³We thank I. Klebanov for reminding us of [48].

2 Preliminaries

Rank-3 tensor models based on fields with 3 indices⁴, ϕ^{abc} , that transform under the symmetry group $O(N)^3$ were introduced in [11]. Here, $a = 1, \dots, N$, $b = 1, \dots, N$, and $c = 1, \dots, N$ are indices that transform in the fundamental representation of each $O(N)$ symmetry group. Similarly, theories based on rank- r indices are constructed out of fields with r indices that transform under the symmetry group $O(N)^r$.

The simplest theories one can define are based on a single tensor-field which is either bosonic or fermionic. Theories with quartic interactions of both types, as well as supersymmetric theories, were introduced, and subsequently studied and generalized in, e.g., [52–67]. In this paper, we focus primarily on sextic interactions, for which it is natural to consider bosonic theories in $d \leq 3$ dimensions, and fermionic theories in $d \leq 1$ (i.e., quantum mechanical models).

A variety of interactions for tensor models exist, which are obtained by contracting the indices in various ways. For example, the wheel interaction [43] is represented by the following interaction term:

$$\mathcal{L}_{\text{wheel}} = \int d^d x \frac{g_{\text{wheel}}}{6} \phi^{a_1 b_1 c_1} \phi^{a_2 b_1 c_2} \phi^{a_2 b_2 c_3} \phi^{a_3 b_2 c_1} \phi^{a_3 b_3 c_2} \phi^{a_1 b_3 c_3}. \quad (2.1)$$

We divide the coupling constant by 6 because that is the size of the automorphism symmetry group of the wheel interaction, as discussed in section 3.2.

One way of drawing Feynman diagrams for the rank-3 tensors is via a triple-line notation that is a straightforward generalization of 't Hooft's double-line notation. Each propagator $\langle \phi^{a_1 b_1 c_1} \phi^{a_2 b_2 c_2} \rangle \sim \delta^{a_1 a_2} \delta^{b_1 b_2} \delta^{c_1 c_2}$ is represented by three coloured lines, with different colours representing the different indices a , b and c ; as shown in Figure 2a. The wheel interaction vertex is represented by the vertex shown in Figure 2b.

A two-loop correction to the propagator is shown in Figure 3. As we will show in section 4, the natural 't Hooft coupling for the wheel is $\lambda_{\text{wheel}} = g_{\text{wheel}} N^3$. In the large N limit, with the 't Hooft coupling fixed, this is a leading-order diagram proportional to λ_{wheel}^2 . This diagram is also an elementary melon. In melonic theories, any leading-order diagrams can be obtained by repeatedly replacing propagators by elementary melons. We will discuss this in more detail in section 5.

For the purpose of systematically enumerating all possible interactions, it is more convenient to represent interactions by an *interaction graph*, as shown in Figure 4. Each vertex in the interaction graph represents a field. Each symmetry group corresponds to a different colour, and coloured edges denote contractions of the corresponding indices. We will refer to the vertices of the interaction graph as *field-vertices*, or simply fields, to avoid confusion with interaction vertices in Feynman diagrams.

⁴An alternative class of tensor models is defined using symmetric traceless or anti-symmetric representations of a single $O(N)$ symmetry group [50, 51]. We do not consider such theories here.

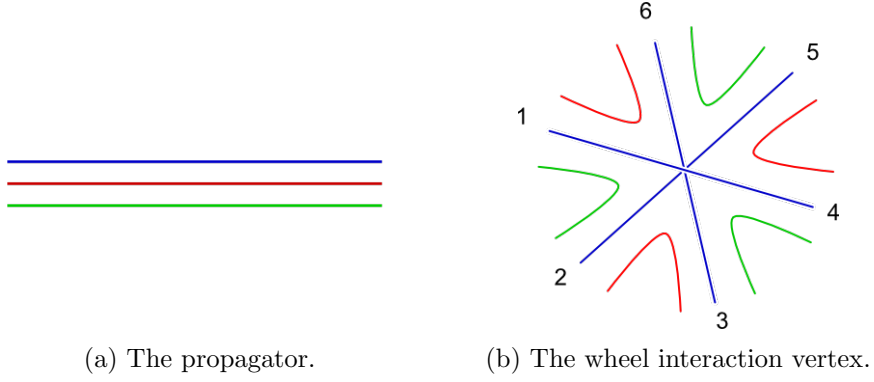


Figure 2: Feynman diagrams in rank-3 tensor models, can be represented by an 3-line notation, with the propagator and interaction vertex as shown above. Each colour corresponds to a different $O(N)$ symmetry group.

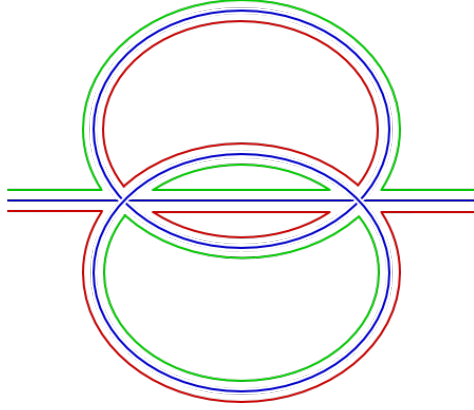


Figure 3: An order g_{wheel}^2 correction to the propagator in triple-line notation. This diagram is also an *elementary melon* and is proportional to $g_{\text{wheel}}^2 N^6 = \lambda_{\text{wheel}}^2$.

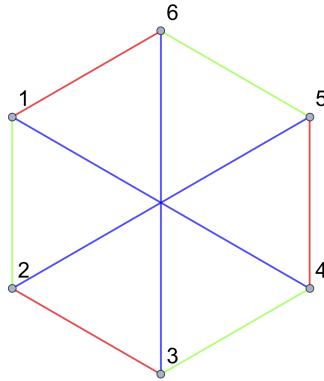


Figure 4: The wheel interaction vertex is represented by the above *labelled interaction graph*.

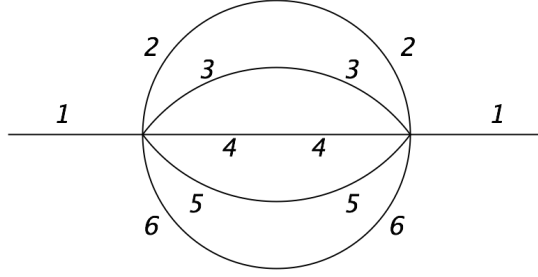


Figure 5: The elementary melon of Figure 3 represented in single-line notation using the field-labels of Figure 4 to specify the Wick contractions.

It is convenient to label the fields-vertices of an interaction graph by $i = 1, 2, \dots, 6$; where p_i represent the momenta of each field, and are “dummy indices”, as can be seen from the momentum-space representation of the vertex:

$$\int \frac{d^d p_1 d^d p_2 d^d p_3 d^d p_4 d^d p_5 d^d p_6}{(2\pi)^{6d}} g \phi(p_1) \phi(p_2) \phi(p_3) \phi(p_4) \phi(p_5) \phi(p_6) \delta^d \left(\sum_i p_i \right). \quad (2.2)$$

Two *labelled interaction graphs* correspond to the same interaction if they can be made identical by a permutation of outgoing-field labels.

Each interaction will be presented with a conventional set of labels for its fields, such as the labels given in Figure 4. One advantage of using these labels is that one can unambiguously represent Feynman diagrams in single-line notation. The elementary melon of Figure 3 can also be represented in single-line notation, using field-labels, as shown in Figure 5.

An interaction graph representing an interaction of rank- r tensors will involve edges of r different colours. Given an interaction graph with r colours, one can remove all edges of a given colour, to obtain an interaction graph with $r - 1$ colours. For example, in Figure 6, if we forget the green edges in the graph on the left, we obtain the 2-colour interaction graph on the right. We call this process “forgetting” a colour. Given an interaction graph, it is convenient to sometimes forget all but 2 colours. We call the resulting interaction graph a two-colour subgraph.

We say that an interaction vertex is *single-trace* if it is represented by a connected interaction graph. An interaction is *maximally-single-trace* (MST) if all its two-colour subgraphs are single-trace [41, 44]. As an example, representatives for all the quartic interaction vertices are pictured in Figure 7. The tetrahedron vertex is maximally-single-trace; the pillow interaction is single-trace, but not maximally-single-trace; and the double-trace interaction is not single-trace.

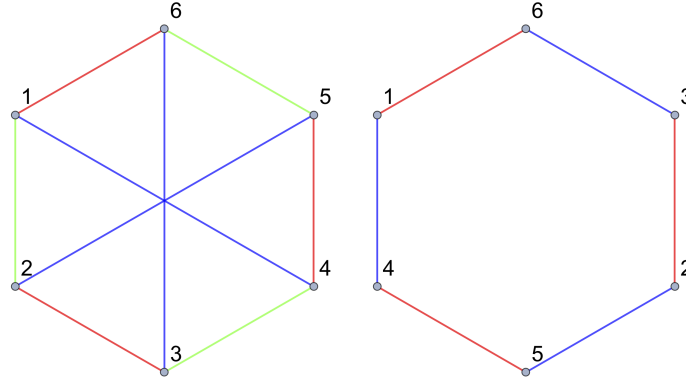
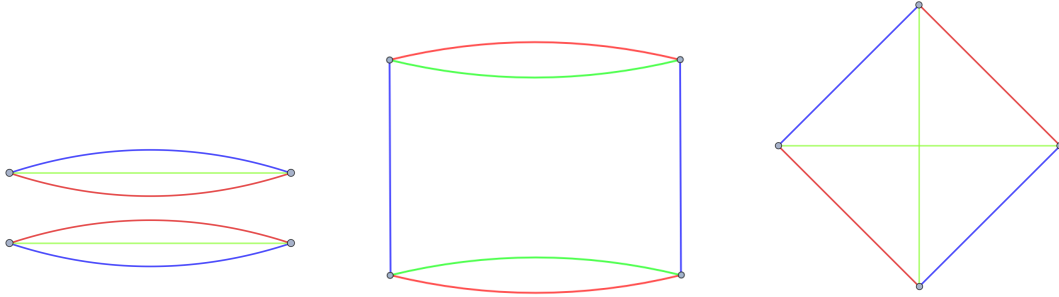


Figure 6: If we “forget” the green edges in the 3-colour interaction graph on the left, we obtain the 2-colour interaction (sub)graph on the right.



(a) A double-trace interaction. (b) The pillow interaction. (c) The tetrahedron interaction.

Figure 7: Representatives of all $r = 3$, $q = 4$ interaction vertices are pictured above. The first interaction on the left is not single-trace, as it is disconnected. The second interaction, the pillow, is single-trace but not maximally-single-trace, because forgetting the blue edges leaves us with a disconnected interaction graph. The last interaction, the tetrahedron, is maximally-single-trace.

3 Sextic maximally-single-trace interactions

The only quartic maximally-single-trace interaction is the tetrahedron. In this section, we enumerate all the sextic maximally-single-trace interactions and discuss their symmetries. Related discussion for tensor models of maximal rank appears in [41, 44].

3.1 Constructing all sextic maximally-single-trace interactions

Here we construct all maximally-single-trace sextic vertices for subchromatic tensor models. For $r = 2$, there is one such vertex, the usual single-trace interaction. Note that this must take form of a connected cyclic graph with edges of alternating colours, which we take to be red and green, as shown in Figure 8.

Let us now consider the $r = 3$ maximally-single-trace interactions. Note that upon

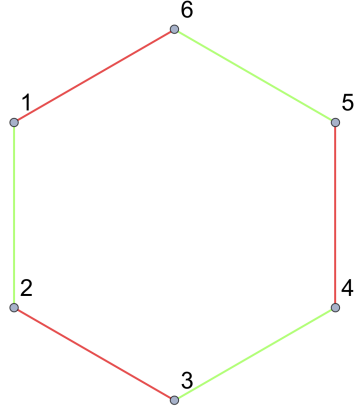


Figure 8: The unique maximally-single-trace interaction vertex for $r = 2$ is represented by a cyclic graph. Any two-colour sub-graph of a Maximally-Single-Trace interaction must be a cyclic graph such as this.

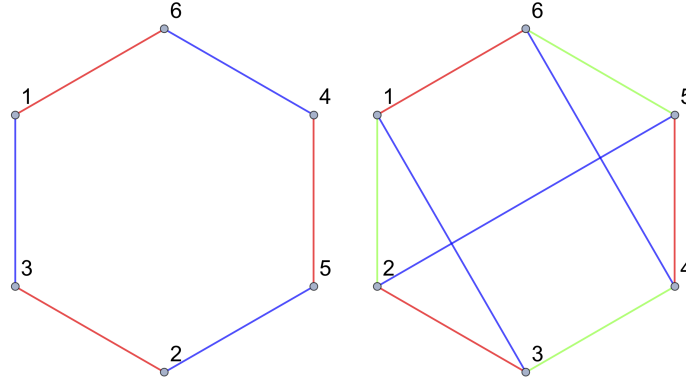


Figure 9: The *prism* interaction vertex, shown on the right, is a maximally-single-trace $r = 3$ interaction that can be obtained from combining the red-green cycle of Figure 8 with the blue-green cycle pictured on the left.

forgetting one colour from an $r = 3$ MST interaction graph, we are left with the $r = 2$ cyclic graph. To construct an $r = 3$ maximally-single-trace interaction, we need to add three blue edges to the red-green cyclic graph of Figure 8, such that the red-blue and green-blue subgraphs are also cyclic graphs. Note that, if we use a blue edge to connect two vertices that were already connected by a green edge, then the blue-green subgraph will consist of two or more disconnected components – hence there are not very many possibilities to consider for the locations of the blue edges. One can explicitly check all possibilities to see that there are exactly two ways to add blue edges which result in an MST interaction – these correspond to the *prism* and the *wheel* shown in Figures 9 and 10.

We will refer to the three colours of the $r = 3$ interactions as (r, g, b) .

Let us now consider the case of $r = 4$. When any one colour is forgotten, the $r = 4$ MST interaction must reduce to a prism or wheel. As before, we consider all ways of adding

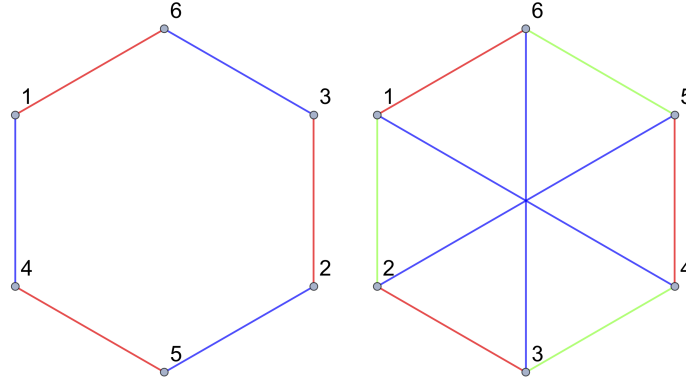


Figure 10: The *wheel* interaction vertex, shown on the right, is a maximally-single-trace $r = 3$ interaction that can be obtained from combining the red-green cycle of Figure 8 with the blue-red cycle pictured on the left.

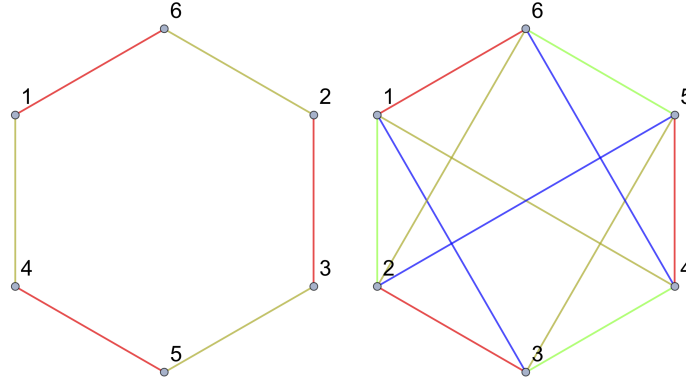


Figure 11: The *double-prism* interaction vertex, shown on the right, is the unique maximally-single-trace $r = 4$ interaction. It can be obtained from combining the $r = 3$ prism interaction of Figure 9 with the yellow-red cycle pictured on the left.

(three) yellow edges to the prism or the wheel, such that the resulting interaction is MST. We find that there is no way of adding yellow edges to the wheel interaction while preserving the MST property; and there is exactly one way to add yellow edges to the prism interaction that preserves MST. Hence there is a unique $r = 4$ MST vertex, depicted in Figure 11. We will refer to the four colours of the $r = 4$ interaction as (r, g, b, y) .

It turns out that one can add a colour to the $r = 4$ MST vertex while preserving the MST property. This gives rise to the unique $r = 5$ MST vertex. This interaction contains the maximal number of colours for a sextic vertex, and gives rise to a traditionally melonic large N limit, as discussed in [44].

This recursive procedure of adding colours to subchromatic graphs can be repeated to enumerate all MST interactions for larger values of q as well.

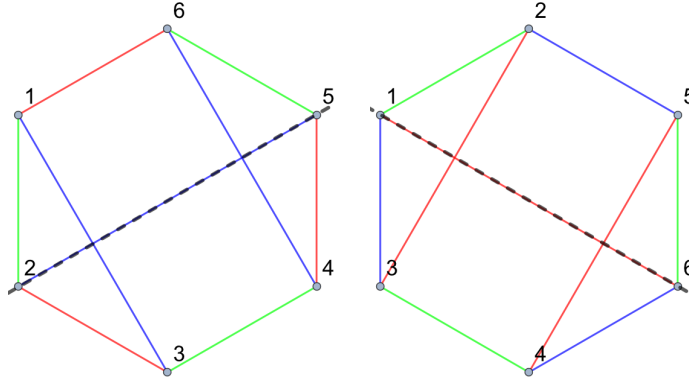


Figure 12: Two ways of drawing the prism interaction graph that make its colour permutation symmetry manifest. Reflection across the dashed line interchanges two colours in each Figure.

3.2 Automorphism and colour permutation symmetry

All of the three MST interactions identified above have a discrete symmetry – they are symmetric under permutation of the $O(N)$ symmetry groups. In terms of the graphical representation of interactions, this is a discrete symmetry under permutation of the various colours in an interaction graph. The interactions may also possess a non-trivial automorphism symmetry group.

We represent symmetry operations by permutations of the field labels in the labelled interaction graph. If a field permutation σ gives rise to a labelled interaction graph isomorphic to the original, σ is an element of the automorphism group of the interaction vertex. If a field permutation σ gives rise to a labelled interaction graph isomorphic to the original graph, up to a permutation of colours, then σ is an element of the colour permutation symmetry group.

In order to show that an interaction is symmetric under all colour permutations, we require that, for each permutation of colours (i.e., relabelling of edges), there is a permutation of field-labels that leaves the labelled interaction graph unchanged. For rank-three interactions, we need to check that all colour permutations which are generated by the two generators $\sigma_{rg} = (r, g)$ and $\sigma_{gb} = (g, b)$, correspond to field-label permutations. For the rank-four interaction, the colour permutation group has 3 generators: σ_{rg} , σ_{gb} , and σ_{by} , and we need to verify that each of these generators corresponds to a permutation of field-labels.

Let us first consider the prism. We draw the prism interaction in two different ways in Figure 12, from which we can see that σ_{rg} is equivalent to the outgoing-field-label permutation $(6, 4)(1, 3)$, and σ_{gb} is equivalent to the vertex permutation $(2, 3)(5, 4)$. We also see that the outgoing-field-label permutation $(1, 6)(2, 5)(3, 4)$ leaves all colours the same. Hence, the prism interaction should conventionally come with a factor of $1/2$ in the Lagrangian.

We next consider the wheel. We draw the wheel in two different ways in Figure 13, from which we can see that σ_{rg} is equivalent to the outgoing-field-label permutation $(1, 5)(2, 4)$,

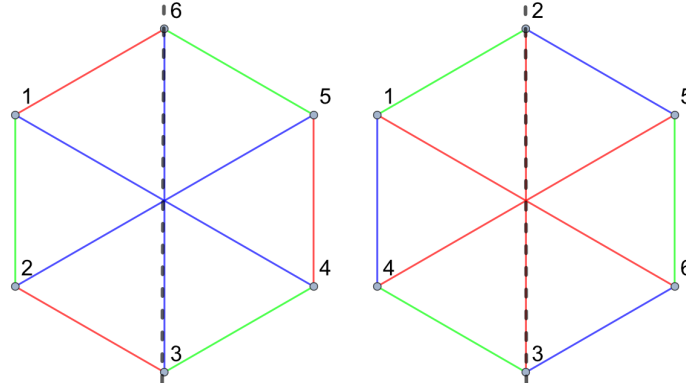


Figure 13: Two ways of drawing the wheel interaction graph. Reflection through the dashed line corresponds to an exchange of two colours.

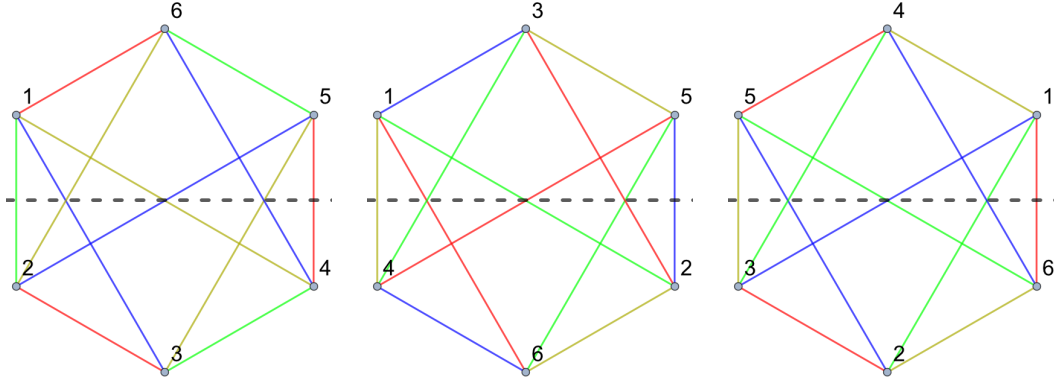


Figure 14: Three ways of drawing the interaction graph for the $r = 4$ double-prism interaction. Reflection through the dashed line corresponds to an exchange of two colours.

and σ_{gb} is equivalent to the field permutation $(1, 5)(4, 6)$. We see that the outgoing-field-label permutations $(1, 6)(2, 5)(3, 4)$ and $(1, 2)(4, 5)(3, 6)$ leave all colours the same. Hence, the wheel interaction should conventionally come with a factor of $1/6$ in the Lagrangian.

Finally, we consider the double-prism. We draw the double-prism in three different ways in Figure 14, from which we can see that σ_{rg} is equivalent to the outgoing-field-label permutation $(1, 4)(2, 5)(3, 6)$, $\sigma_{gb} = (1, 6)(2, 4)(3, 5)$, and $\sigma_{by} = (1, 2)(3, 6)(4, 5)$. There is no outgoing-field-label permutation that leaves all colours the same, so the interaction comes with a factor of 1 in the Lagrangian.

Let us conclude this section with the observation that, if the automorphism symmetry group includes a field-label permutation that is odd, then the 1-dimensional fermionic interaction term based on that interaction vanishes in a theory of Majorana fermions, due to anti-commutation of Grassmann variables.

In particular, as observed in [40], for the wheel:

$$L_{\text{wheel}} = \frac{g_{\text{wheel}}}{6} \int dt \psi^{a_1 b_1 c_1} \psi^{a_1 b_2 c_2} \psi^{a_2 b_2 c_3} \psi^{a_2 b_3 c_1} \psi^{a_3 b_3 c_2} \psi^{a_3 b_1 c_3} \quad (3.1)$$

$$= -\frac{g_{\text{wheel}}}{6} \int dt \psi^{a_3 b_1 c_3} \psi^{a_3 b_3 c_2} \psi^{a_2 b_3 c_1} \psi^{a_2 b_2 c_3} \psi^{a_1 b_2 c_2} \psi^{a_1 b_1 c_1} \quad (3.2)$$

$$= -L_{\text{wheel}}. \quad (3.3)$$

In the second line, we applied the field permutation $(1, 6)(2, 5)(3, 4)$. In the third line, because this is an automorphism, we are able to relabel the dummy indices a_i , b_i and c_i (via: $a_3 \leftrightarrow a_1$, $b_2 \leftrightarrow b_3$) to undo this permutation. Similarly, for the prism:

$$L_{\text{prism}} = \frac{g_{\text{prism}}}{2} \int dt \psi^{a_1 b_1 c_1} \psi^{a_1 b_2 c_2} \psi^{a_2 b_2 c_1} \psi^{a_2 b_3 c_3} \psi^{a_3 b_3 c_2} \psi^{a_3 b_1 c_3} \quad (3.4)$$

$$= -\frac{g_{\text{prism}}}{2} \int dt \psi^{a_3 b_1 c_3} \psi^{a_3 b_3 c_2} \psi^{a_2 b_3 c_3} \psi^{a_2 b_2 c_1} \psi^{a_1 b_2 c_2} \psi^{a_1 b_1 c_1} \quad (3.5)$$

$$= -L_{\text{prism}}. \quad (3.6)$$

These arguments do not apply to complex fermions.⁵

Let us also remark that, if we would like to define a theory with complex fields, and promote all the symmetry groups to $U(N)$, then we require the interaction graph to be bipartite. The wheel is bipartite, but the prism, double-prism and triple prism are not bipartite. If we wish to promote some, but not all, of the symmetry groups to $U(N)$, this restriction does not apply.

In all cases, real bosonic versions of these theories can be defined, and can be thought of as special cases of the general sextic bosonic theory studied perturbatively in [68].

4 Large N limit of sub-chromatic maximally-single-trace interactions

We now consider the large N limit of the maximally-single-trace interaction vertices defined in the previous section. In this section we present results for an arbitrary maximally-single-trace interaction of any order q . We follow the approach outlined in [11].

4.1 Large N scaling of coupling constants

Let us first determine the natural scaling of the coupling constant with N , in the large N limit, for an order- q maximally-single-trace interaction with r indices.

Consider a connected Feynman diagram with no external edges, i.e., one that contributes to the free energy of our theory. As shown in the previous sections, Feynman diagrams

⁵We thank I. Klebanov for discussions on this point.

for fields based on rank- r tensors can be drawn in a multi-line notation, using r different colours. If we take any such diagram, and erase all but two of the colours, we obtain what is known as a *fat sub-graph*. Since our multi-line propagator contains r colours, we can generate $r(r-1)/2$ fat sub-graphs – one for each pair of colours. We shall use the index α , where $\alpha = 1, \dots, r(r-1)/2$, to label each of these fat graphs. We denote the number of loops for each fat graph by f_α . Then, summing over all such pairs of indices, we obtain,

$$\sum_{\alpha=1}^{r(r-1)/2} f_\alpha = (r-1)f_{total}, \quad (4.1)$$

where f_{total} is the total number of loops in the graph and determines the power of N .

Because our interaction vertices are maximally-single-trace, each fat graph will consist of a single connected component. The Euler equation for each α can be written as,

$$f_\alpha + v - e = \chi_\alpha = 2 - 2g_\alpha \quad (4.2)$$

where v and e refer to the number of vertices and edges in the graph (which are the same for all fat sub-graphs) and g_α is the genus of the fat graph labelled by α . For *maximal* graphs with the largest power of N , we require all fat graphs to be planar, and $g_\alpha = 0$.

Since our vertices are order- q , we have $2e = qv$. Placing this into the above equation, we obtain,

$$\begin{aligned} f_\alpha + v \left(1 - \frac{q}{2}\right) &= 2 - 2g_\alpha \\ f_\alpha + v \left(1 - \frac{q}{2}\right) &\leq 2 \end{aligned} \quad (4.3)$$

Now, summing over all α , we get

$$\begin{aligned} \sum_{\alpha=1}^{r(r-1)/2} f_\alpha + \sum_{\alpha=1}^{r(r-1)/2} v \left(1 - \frac{q}{2}\right) &\leq 2 \sum_{\alpha=1}^{r(r-1)/2} 1 \\ (r-1)f_{tot} + \frac{r(r-1)}{2} v \left(1 - \frac{q}{2}\right) &\leq r(r-1) \end{aligned} \quad (4.4)$$

which imply,

$$f_{tot} \leq \frac{r}{4}(q-2)v + r. \quad (4.5)$$

We define *maximal* Feynman graphs to be those that contain the largest number of loops, or equivalently, give rise to only planar fat-graphs. Maximal graphs, therefore saturate the above bound, satisfying the relation:

$$f_{tot} = \frac{r}{4}(q-2)v + r. \quad (4.6)$$

This relation tells us that we should define the large N limit while keeping the 't Hooft coupling

$$\lambda = gN^{r(q-2)/4}, \quad (4.7)$$

fixed. Then, the free energy scales with N as,

$$N^r f(\lambda). \quad (4.8)$$

4.2 Existence of a loop passing through one or two vertices

We now show that any connected maximal diagram contributing to the free energy contains a loop passing through exactly one vertex or a loop passing through exactly two vertices. Let us define \mathcal{F}_s to be the number of loops passing through s vertices [11]. Clearly,

$$\sum_{s=0}^{\infty} \mathcal{F}_s = f_{total} \quad (4.9)$$

Also, by considering the total number of coloured lines passing through a vertex in the multi-line notation, one can see that:

$$\sum_{s=1}^{\infty} s\mathcal{F}_s = rq\frac{v}{2}. \quad (4.10)$$

Combining (4.9) and (4.10), and eliminating f_{total} using (4.6), we obtain

$$\sum_s \left(\frac{2q}{(q-2)} - s \right) \mathcal{F}_s = \frac{2q}{(q-2)} r. \quad (4.11)$$

When $q \geq 6$, one can separate the terms \mathcal{F}_1 and \mathcal{F}_2 from the sum, to obtain the following inequality:

$$(q+2)\mathcal{F}_1 + 4\mathcal{F}_2 \geq 2qr. \quad (4.12)$$

Thus, for any free energy graph, there is at least one loop passing through one vertex, or one loop passing through two vertices.⁶

We refer to loops passing through one vertex as *1-cycles*. While 1-cycles may not contribute to a physical calculation, we will still keep the possibility of their existence open in what follows, as we are only interested in obtaining the restrictions that follow from purely combinatorial considerations.

We refer to a loop passing through two vertices as a *2-cycle*. The existence of a 2-cycle itself is not enough to guarantee a large N limit dominated by melonic diagrams.

⁶The above analysis assumed that the number of interaction vertices was greater than or equal to 1. The trivial free-energy diagram which contains no interaction vertices, is also maximal.

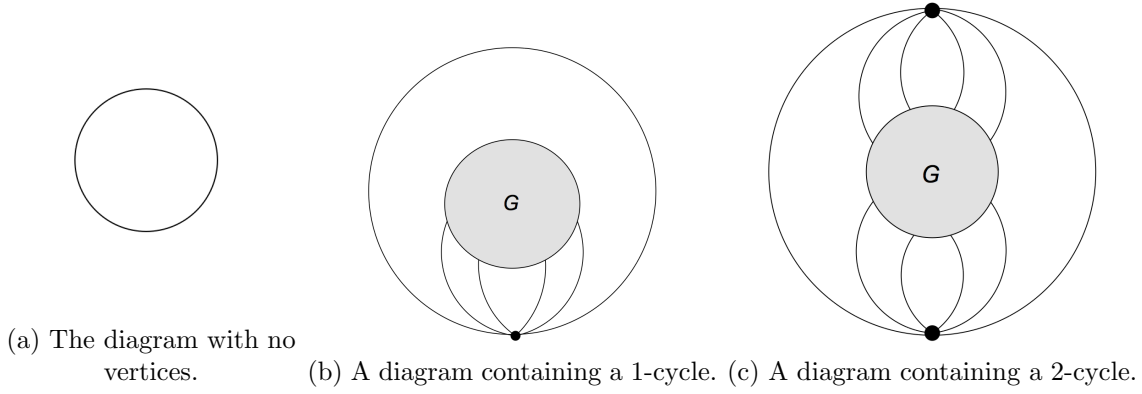


Figure 15: Any maximal Feynman diagram contributing to the free energy must be of one of the three types specified above. To obtain a recursive enumeration of all Feynman diagrams, we must place some constraints on the subgraph G .

5 Melonic dominance of subchromatic interaction vertices

Here, we consider specific theories based on the sextic maximally-single-trace interactions listed above. We can consider a theory with $r = 3$, which may contain a wheel interaction, a prism interaction, or both. We can also consider a theory with $r = 4$, for which the only interaction is the double prism. (The theory for $r = 5$ was discussed in [44] so we do not discuss it here.) We wish to explicitly enumerate the maximal Feynman diagrams that contribute to the free energy in any such theory. Our arguments are inspired by [41, 44, 69].

Our strategy is as follows. In the previous section, we showed that any Feynman diagram contributing to the free energy that survives in the large N limit must either:

1. Contain no vertices, in which case it is just the zeroth-order diagram.
2. Contain at least one 1-cycle.
3. Contain at least one 2-cycle.

These cases are illustrated in Figure 15. To enumerate all the maximal Feynman diagrams contributing to the free energy, we need to enumerate all the in-equivalent 1-cycles and 2-cycles. For each in-equivalent 2-cycle and 1-cycle, we draw each of its $r(r-1)/2$ fat graphs, and impose the restriction that each fat graph is planar.

When we draw a fat graph corresponding to a particular pair of colours, we must arrange the outgoing lines from each interaction vertex in a particular cyclic order, for the graph to be manifestly planar. For example, consider the wheel interaction, shown in Figure 22. If we draw a blue red fat-graph, we must arrange the outgoing lines in the cyclic order 163254 (or 145236). If we instead draw a red-green fat-graph, we must arrange the outgoing lines in the cyclic order 123456 (or 654321).

For a given pair of colours, the requirement of fat-graph planarity might rule out a particular 2-cycle entirely, such as for the 2-cycle shown in Figure 16. Alternatively, this requirement

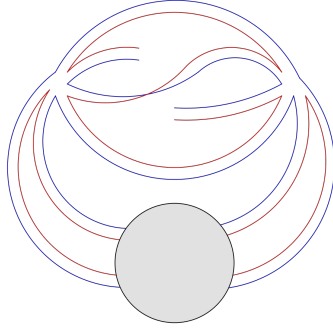


Figure 16: A 2-cycle which contains a twist in and is therefore non-planar.

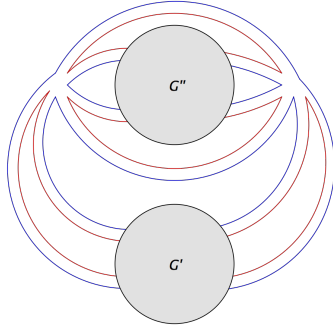


Figure 17: We require each two-colour fat graph to be planar. For a given choice of two-colours, such as red and blue, planarity forces us to arrange the outgoing edges from each interaction vertex in a particular cyclic order. This means that the 2-cycle may split the subgraph G from Figure 15c into two disconnected pieces, as shown above. If we consider all two-colour fat graphs, we hope to split the graph G into four disconnected pieces as shown in Figure 18.

would “divide” the subgraph G into two smaller disconnected components G' and G'' as shown in Figure 17.

Suppose the requirement of fat-graph-planarity splits the subgraphs G of Figure 15b and 15c into disconnected components, as shown in Figure 18, for each inequivalent 1-cycle and 2-cycles. Crucially, each of these sub-graphs contains only two external edges. This allows us to use a cutting and sewing argument to isolate the graphs $G^{(i)}$, as shown in Figure 19. Each of the cut-and-sewn subgraphs $G^{(i)}$ defines a maximal Feynman diagram contributing to the free energy, and the arguments of this section apply to the cut-and-sewn subgraph as well. We have thus obtained a recursive enumeration of all the Feynman diagrams contributing to the free energy.

Melonic moves

One can convince oneself that the set of maximally free energy diagrams enumerated by this recursive procedure above can also be obtained starting from the 0-cycle by repeatedly

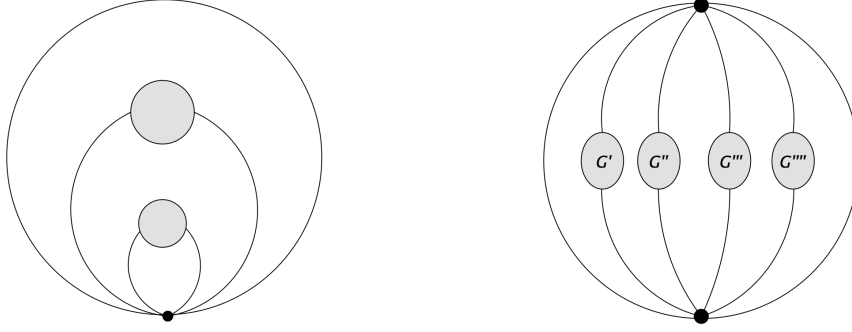
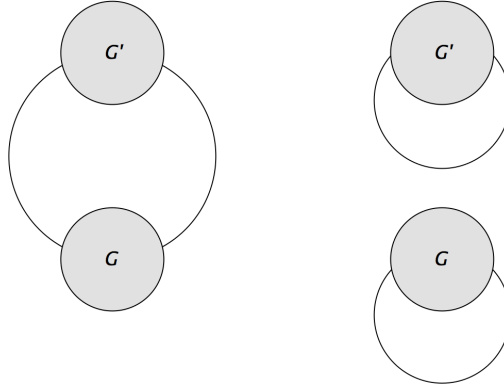


Figure 18: If, for all possible 1-cycles and 2-cycles, the requirement that all two-colour fat graphs are planar splits up the subgraph G from Figure 15b and 15c into disconnected components as shown above, then we can argue the theory is melonic the conventional sense, via the cutting and sewing argument in Figure 19.



(a) The “connectivity structure” of a connected graph with two external edges must be the same as that of a free propagator.



(b) We can argue that the combined graph of G and G' on the left is maximal if and only if both separated components on the right are maximal, since each subgraph can be replaced by a free propagator without affecting the N counting.

Figure 19: The above two Figures illustrate a cutting and sewing argument that can be used to separate the graphs G' , G'' , G''' and G'''' from Figure 18. Either these graphs contain no vertices, or they contain a 1-cycle or 2-cycle. One thus obtains a recursive characterization of all the leading order graphs.

replacing propagators by “elementary snails” or “elementary melons” as shown in Figure 20. We refer to the diagrams obtained by this sort of recursive procedure as *melon diagrams*.

The set of all elementary melons can be obtained from the list of maximal free-energy graphs containing a 2-cycle: we first replace all subgraphs (shaded blobs) by free propagators, and then cut any one of the edges open to obtain an elementary melon such as the one shown in Figure 20. The set of all elementary snails can be obtained from the list of maximal free energy graphs containing a 1-cycle in a similar manner.

The act of replacing a propagator by an elementary snail or elementary melon is called an elementary melonic move. It is easy to see that, in general, the act of replacing a propagator by an elementary melon causes $v \rightarrow v + 2$ and $f_{tot} \rightarrow f_{tot} + \frac{r}{2}(q - 2)$. We also have a similar result for the elementary snail. Hence, elementary melonic moves preserve (4.6), so all melonic graphs are maximal. However, to show that all maximal graphs are melonic requires us to carry out the argument given above; recursively enumerate all free-energy diagrams via analysis of 1-cycles and 2-cycles.

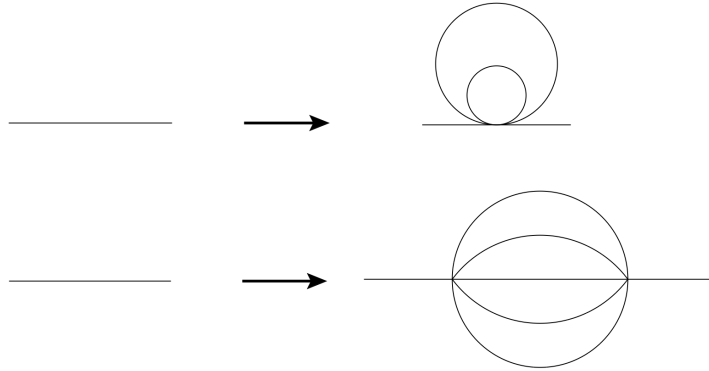


Figure 20: The diagrams recursively enumerated via the argument in the text can also be generated by repeatedly replacing propagators with an elementary snail (above) or an elementary melon (below). The snail need not be present in all models,

This translates into the following equation for the exact propagator shown in Figure 21. The snails may or may not be present depending on the interaction. As mentioned earlier, the snails are tadpoles, and would formally vanish in a quantum field theory due to dimensional regularization.

Let us conclude this section with the caveat that, while it is straightforward to obtain the Schwinger-Dyson equation for the exact propagator, if one wants to actually evaluate the free energy, one must also include the symmetry factors for each of these diagrams. As one can see from the diagrammatic expansion for the free energy in a vector model, e.g., [70], these factors are generally non-trivial.

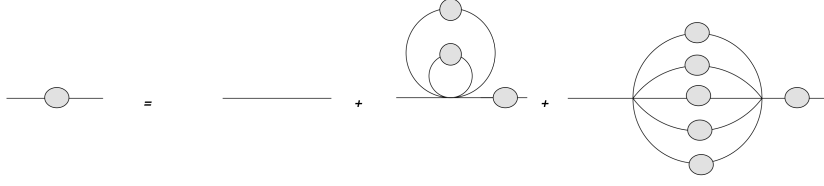
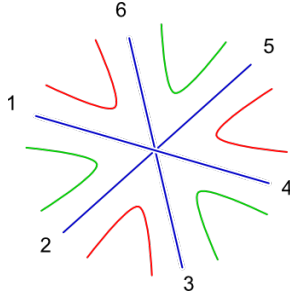


Figure 21: The melonic moves give rise to the above schematic equation for the exact propagator. If one were to connect the two external lines together, the first term on the RHS is a 0-cycle, the second term is a 1-cycle, and the third term is a 2-cycle.

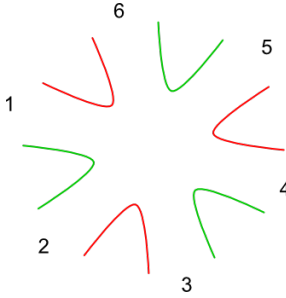
5.1 Wheel

In this section we demonstrate the melonic dominance of the wheel vertex, according to the general recipe above.

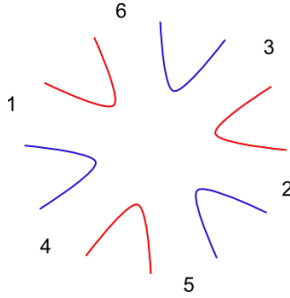
The wheel vertex is shown in Figure 22, along with its three two-colour fat vertices.



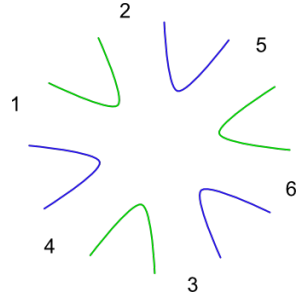
(a) The wheel interaction is shown as a triple-line fat vertex.



(b) The red-green fat vertex.



(c) The red-blue fat vertex.



(d) The green-blue fat vertex.

Figure 22: The wheel interaction and its three two-colour fat-vertices are shown above. For a given choice of two-colours, we must arrange the labelled-fields in one of the two particular cyclic orders in order to maintain manifest planarity.

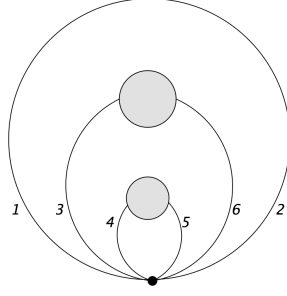


Figure 23: Any Feynman diagram containing a loop passing through one wheel vertex must be of this form, or related to this by permutation of colours.

5.1.1 1-cycles

A 1-cycle is formed by contracting two fields from the same interaction vertex, which we denote as $\langle X, Y \rangle$. Using the automorphism symmetry of the wheel interaction, we can always choose the first field $X = 1$. Via colour permutation symmetry, the second field Y can be chosen to be 2 or 3. There are thus two possible 1-cycles, one has to consider $\langle 1, 2 \rangle$ and $\langle 1, 3 \rangle$.

The 1-cycle $\langle 1, 3 \rangle$ results in a non-planar red-green fat graph, and hence is non-maximal.

The $\langle 1, 2 \rangle$ 1-cycle is constrained to be of the form in Figure 23.

5.1.2 2-cycles

A 2-cycle is specified by two Wick contractions. We label the two interaction vertices L and R ; each Wick contraction must include one field from each interaction vertex. We thus specify the two Wick contractions that define the 2-cycle in the following notation: $(\langle X_L, Y_R \rangle, \langle Z_L, W_R \rangle)$, where X, Y, Z , and W are integers between 1 and 6 corresponding to the field labels given in the labelled interaction graph of Figure 10. The notation means that field from the left interaction vertex labelled by the number X in the labelled interaction graph is contracted with the field labelled by the number Y from the right interaction vertex. [44]

A priori there are a large number of different 2-cycles that are possible. However, using the automorphism and colour permutation symmetries of the wheel interaction, we can reduce the total number of inequivalent 2-cycles to a very manageable number. The idea behind this is that if a particular 2-cycle $(\langle X_L, Y_R \rangle, \langle Z_L, W_R \rangle)$ induces only planar fat graphs, then the same must be true for any other 2-cycle $(\langle X'_L, Y'_R \rangle, \langle Z'_L, W'_R \rangle)$ obtained by a permutation of colours. Hence we do not need to check all different 2-cycles: we only need to check the subset of 2-cycles whose orbit under the colour permutation (and automorphism) symmetry group covers all 2-cycles. This is an elementary exercise in group theory, which, for the sake of clarity and completeness we spell out explicitly in the appendix.

As shown in the appendix, the inequivalent 2-cycles are

1. $(\langle 1_L, 1_R \rangle, \langle 2_L, W_R \rangle)$,

2. $(\langle 1_L, 1_R \rangle, \langle 3_L, W'_R \rangle)$,

where $W_R = 2, 3$ or 4 , and $W'_R = 2, 3$ or 5 .

If W_R is odd, or if W'_R is even, one can check that the red-green fat graph arising from this loop contains a twist, and hence is non-planar. Hence there are only four different 2-cycles to consider.

Let us first consider the 2-cycle $(\langle 1_L, 1_R \rangle, \langle 2_L, 2_R \rangle)$. The three fat graphs for this loop are shown in Figure 24. Using these constraints we have two possibilities for the 2-cycle, shown in Figure 25.

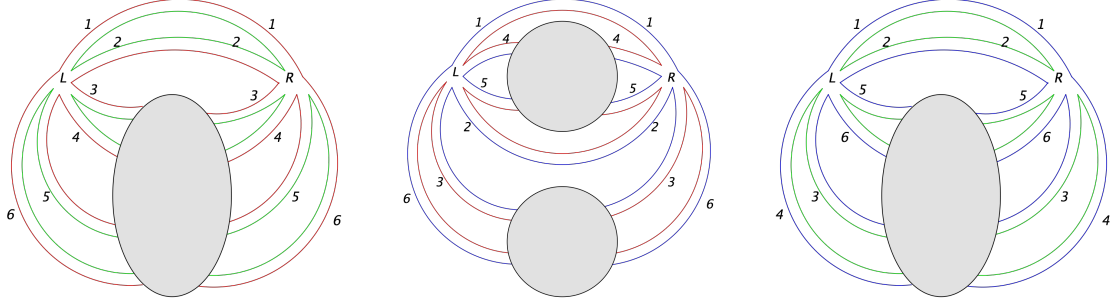


Figure 24: The fat graphs for the loop $(\langle 1_L, 1_R \rangle, \langle 2_L, 2_R \rangle)$ involving two wheel interaction vertices. From the blue-red fat-graph, we see that 4_L can be connected (via a subgraph) to one of $4_R, 5_R$ or 5_L . If 4_L is connected to 4_R or 5_R , then we see from the red-green fat graph that 3_L must be connected to 3_R , and 6_L must be connected to 6_R . Then using the blue-green fat-graph, we see 4_L must be connected to 4_R and 5_L must be connected to 5_R . This corresponds to the first graph on the left in Figure 25. If, instead, 4_L is connected to 5_L , one can similarly work out that the connections must be as depicted in the second graph in Figure 25.

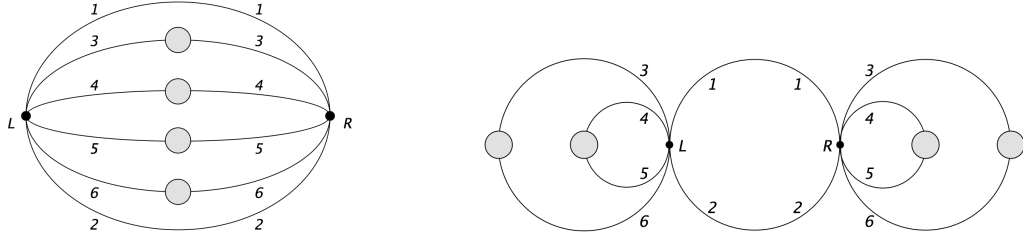


Figure 25: For the loop $(\langle 1_L, 1_R \rangle, \langle 2_L, 2_R \rangle)$, the constraint that all fat graphs are planar means the interaction vertices must be connected in one of the two above ways. The second possibility is a “double-snail” that originates from the insertion two elementary snails.

For the 2-cycle $(\langle 1_L, 1_R \rangle, \langle 2_L, 4_R \rangle)$, the results consistent with planarity of fat-graphs are shown in Figure 26.

Let us next consider the loop $(\langle 1_L, 1_R \rangle, \langle 3_L, 3_R \rangle)$. The three fat graphs for this loop are shown in Figure 27. Using these constraints we have the following two possibilities for the 2-cycle:

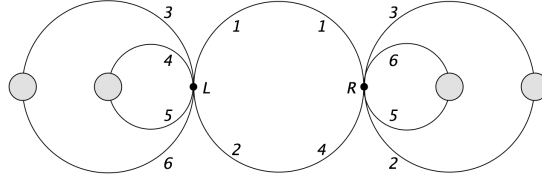


Figure 26: For the loop $(\langle 1_L, 1_R \rangle, \langle 2_L, 4_R \rangle)$ connecting two wheel interaction vertices, the constraint that all fat graphs are planar means the interaction vertices must be connected as shown above.

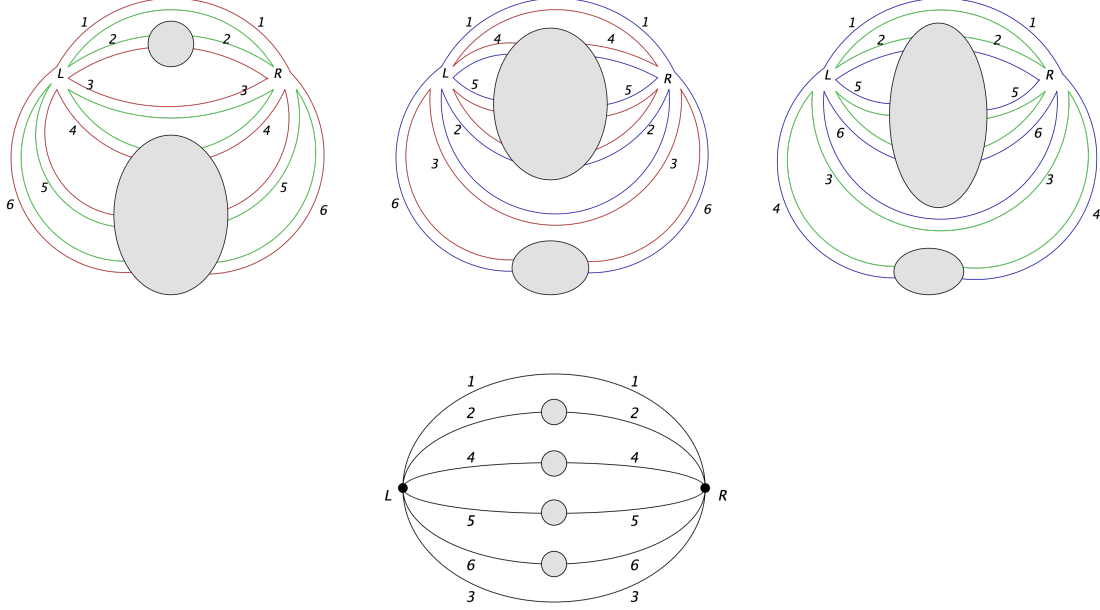


Figure 27: For the loop $(\langle 1_L, 1_R \rangle, \langle 3_L, 3_R \rangle)$ connecting two wheel interaction vertices, the constraint that all fat graphs (shown above) are planar means the interaction vertices must be connected as shown below.

For the 2-cycle $(\langle 1_L, 1_R \rangle, \langle 3_L, 5_R \rangle)$, we find there is no way to satisfy the constraints that all fat-graphs be planar.

From the in-equivalent 1-cycles and 2-cycles above, we can extract the elementary melon and elementary snail shown in Figure 28.

5.2 $r = 4$ Double-prism

Let us now consider the double-prism. (we consider this case before the prism, because it also gives rise to a conventional melonic limit.) Its fat vertices are pictured in Figure 29.

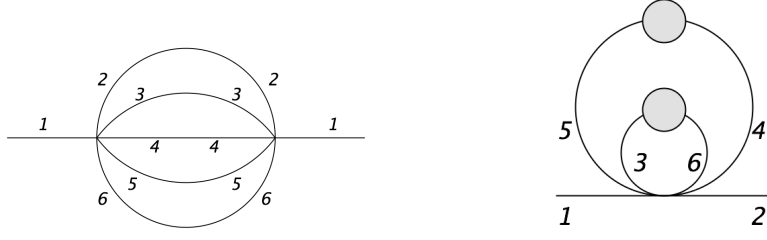


Figure 28: The maximal diagrams arising from the wheel interaction can also be generated by replacing propagators with the above elementary snail and elementary melon (or their colour permutations).

5.2.1 1-cycles

One can check that, for the double-prism, there is no way of forming a 1-cycle such that all six fat-graphs are planar. Hence elementary snails are ruled out on purely combinatorial grounds.

5.2.2 2-cycles

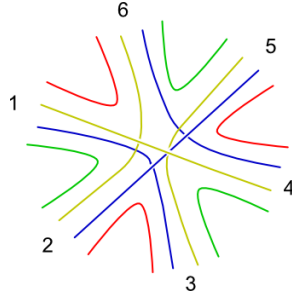
Let us enumerate all in-equivalent 2-cycles: $(\langle X_L, Y_R \rangle, \langle Z_L, W_R \rangle)$ passing through two double-prism interaction vertices.

The double-prism has no automorphism symmetry. However, we can use the colour permutation symmetry to reduce the number of cases one has to check to ensure all fat-graphs are planar.

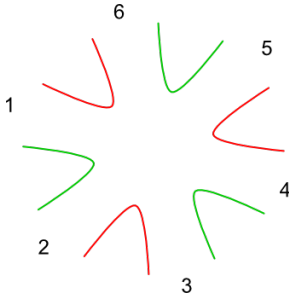
By permuting the colours in the Feynman diagram, any loop can be mapped to one in which $X = 1$. This procedure does not use all the colour permutation symmetry, as the permutation $\sigma_{(gbyr)}$ corresponds to the field-vertex permutation $(2, 3, 4, 6)$, which leaves the choice of $X = 1$ invariant. In case Y was chosen to be 3, 4 or 6, one could use the colour permutation $\sigma_{(gbyr)}$ to map it to an equivalent diagram where $Y = 2$. We can thus set $Y = 1, 5$ or 2. If $Y = 1, 5$, then the colour permutation symmetry still remains at our disposal to set $Z = 1, 5$ or 2. Finally, if $Z = 1, 5$, the unused colour permutation symmetry can be used set $W = 1, 5$ or 2.

The in-equivalent 2-cycles can then be taken to be:

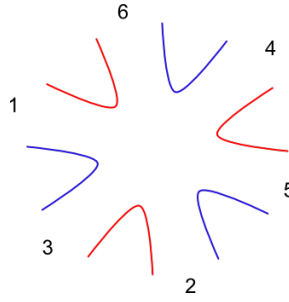
1. $(\langle 1_L, 2_R \rangle, \langle Z_L, W_R \rangle)$
2. $(\langle 1_L, 5_R \rangle, \langle 2_L, W'_R \rangle)$
3. $(\langle 1_L, 5_R \rangle, \langle 5_L, 2_R \rangle)$
4. $(\langle 1_L, 5_R \rangle, \langle 5_L, 1_R \rangle)$
5. $(\langle 1_L, 1_R \rangle, \langle 2_L, W''_R \rangle)$
6. $(\langle 1_L, 1_R \rangle, \langle 5_L, 5_R \rangle)$



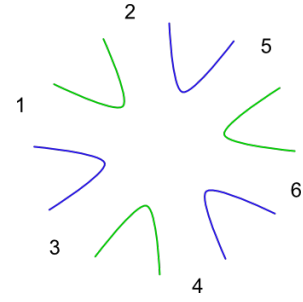
(a) The double-prism interaction as a multi-line fat vertex.



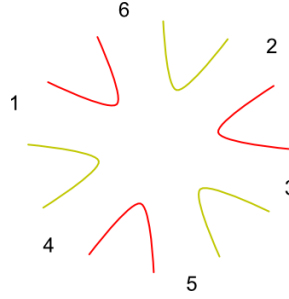
(b) The red-green fat vertex.



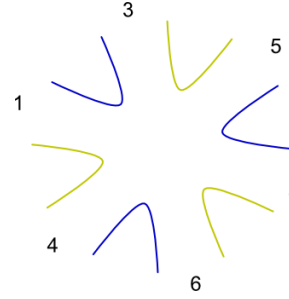
(c) The red-blue fat vertex.



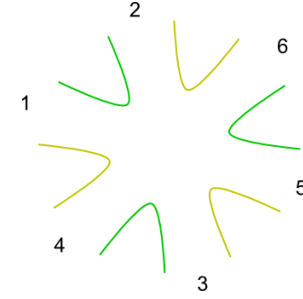
(d) The blue-green fat vertex.



(e) The yellow-red fat vertex.



(f) The blue-yellow fat vertex.



(g) The yellow-green fat vertex.

Figure 29: The double-prism interaction and its three two-colour fat-vertices are shown above. Note that, for a given choice of two-colours, we must arrange the fields in a particular cyclic order in order to maintain manifest planarity

The condition of no twists for fat-graphs forces $W'' = 2$, $Z = 2$, $W = 1$. It also rules out case 2 and 3. Thus there are only four possibly-planar inequivalent 2-cycles, which are:

- $(\langle 1_L, 2_R \rangle, \langle 2_L, 1_R \rangle)$
- $(\langle 1_L, 5_R \rangle, \langle 5_L, 1_R \rangle)$
- $(\langle 1_L, 1_R \rangle, \langle 2_L, 2_R \rangle)$
- $(\langle 1_L, 1_R \rangle, \langle 5_L, 5_R \rangle)$

Drawing all fat-graphs, we find that there is no way to make the loops $(\langle 1_L, 2_R \rangle, \langle 2_L, 1_R \rangle)$, or $(\langle 1_L, 5_R \rangle, \langle 5_L, 1_R \rangle)$, part of a diagram that is planar for all fat-graphs.

Next we draw all fat graphs for $(\langle 1_L, 1_R \rangle, \langle 5_L, 5_R \rangle)$. Requiring all fat graphs to be planar gives rise to a traditional 2-cycle, with vertex i_R paired with vertex i_L , shown in Figure 30. A similar result holds for $(\langle 1_L, 1_R \rangle, \langle 2_L, 2_R \rangle)$.

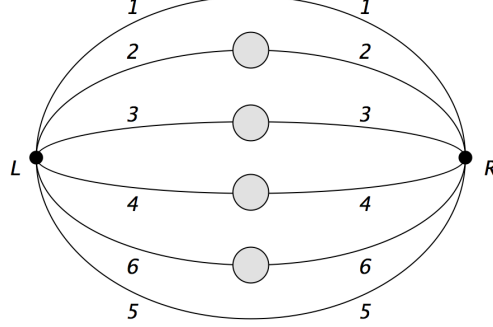


Figure 30: Requiring the 2-cycle $(\langle 1_L, 1_R \rangle, \langle 5_L, 5_R \rangle)$ to be maximal means it must take the above traditionally-melonic form. A similar result holds for $(\langle 1_L, 1_R \rangle, \langle 2_L, 2_R \rangle)$.

Putting all these results together, we find that this model is melonic in the conventional sense. All diagrams can be generated by replacing propagators by the elementary melon shown below in Figure 31. There is no elementary snail, unlike the case of the wheel.

5.3 $r = 3$ Prism

The prism interaction and its two-colour fat vertices, are shown in Figure 32. In [43], it was shown that the leading order diagrams arising from the prism interaction can be explicitly summed by using an auxiliary field to convert it into a quartic tetrahedron interaction, for which melonic dominance is well-known.

However, if we do not introduce this auxiliary field, and simply draw Feynman diagrams using the sextic prism vertex, we find that there are maximal diagrams which are not melonic in the sextic sense. In other words, the set of maximal Feynman diagrams in the prismatic

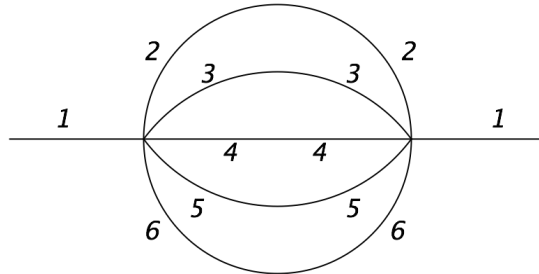
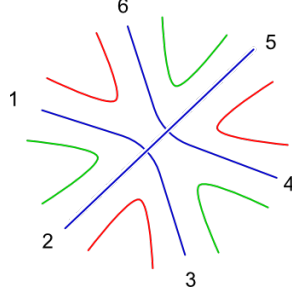


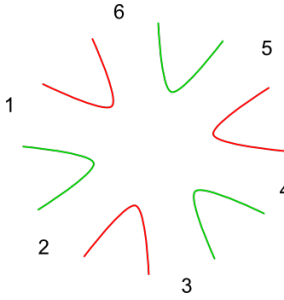
Figure 31: The theory based on the double-prism is traditionally melonic, with the above elementary melon (and its colour permutations).

theory includes diagrams that would not be maximal in a conventional melonic theory, such as a theory based on the double-prism or a theory based on the $r = 5$ maximally-single-trace interaction studied in [44]. An example of such a diagram is shown in Figure 1.

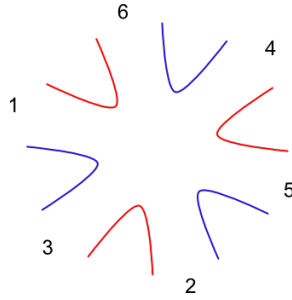
Because the prism interaction gives rise to a large N limit, it is not conventionally melonic in this sense. It is interesting to see how the method of analysis given above can be modified for this case.



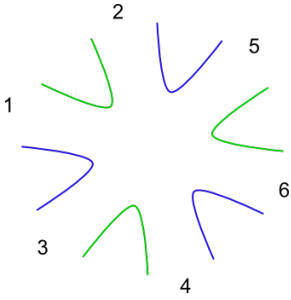
(a) The prism interaction is shown as a triple-line fat vertex.



(b) The red-green fat vertex for the prism.



(c) The red-blue fat vertex for the prism.



(d) The blue-green fat vertex for the prism.

Figure 32: The prism interaction and its three two-colour fat-vertices are shown above. Note that, for a given choice of two-colours, we must arrange the fields in a particular cyclic order in order to maintain manifest planarity

5.3.1 1-cycles

One can check that the only maximal Feynman diagram containing a 1-cycle is $\langle 1, 6 \rangle$, or its colour permutations. It takes the form shown in Figure 33.

5.3.2 2-cycles

Consider two prism interaction vertices, one denoted by L and the other R . In order to specify a 2-cycle, we again have to specify the following contractions: $(\langle X_L, Y_R \rangle, \langle Z_L, W_R \rangle)$.

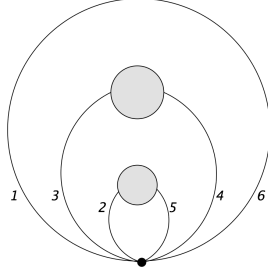


Figure 33: Any maximal Feynman diagram containing a loop passing through one prism vertex must be of this form, or related to this by permutation of colours.

We can choose $X_L = 1_L$ using the automorphism of the first interaction vertex and the colour permutation symmetry. The automorphism symmetry of the second vertex and the residual colour permutation symmetry group (which leaves 1 invariant) can be used to choose $Y_R = 1_R$ or 2_R . If $Y_R = 1_R$ the residual colour permutation symmetry can be used to set $Z_L = 2_L, 4_L$, or 6_L . Thus, we have the following in-equivalent 2-cycles,

1. $(\langle 1_L, 1_R \rangle, \langle Z_L, W_R \rangle)$
2. $(\langle 1_L, 2_R \rangle, \langle Z'_L, W'_R \rangle)$

where $Z = 2, 4, 6$.

The condition of no-twists-in-fat-graphs then restricts the allowed 2-cycles to be:

1. $(\langle 1_L, 1_R \rangle, \langle 2_L, 2_R \rangle)$
2. $(\langle 1_L, 1_R \rangle, \langle 4_L, 4_R \rangle)$
3. $(\langle 1_L, 1_R \rangle, \langle 6_L, 6_R \rangle)$
4. $(\langle 1_L, 2_R \rangle, \langle 2_L, 1_R \rangle)$
5. $(\langle 1_L, 2_R \rangle, \langle 5_L, 6_R \rangle)$

Let us look at the structure of the fat graphs produced by these contractions. First, one can check that the 2-cycle $\langle 1_L, 2_R \rangle, \langle 5_L, 6_R \rangle$ and $\langle 1_L, 2_R \rangle, \langle 2_L, 1_R \rangle$ always give rise to a non-planar fat graph.

Next consider the case $(\langle 1_L, 1_R \rangle, \langle 4_L, 4_R \rangle)$. Using the planarity of the fat sub-graphs, we just have the conventional melonic diagram, as shown in Figure 34.

We then consider the case $\langle 1_L, 1_R \rangle, \langle 6_L, 6_R \rangle$. For this contraction, we observe either a conventional melonic diagram, or a double-snail.

We finally consider $(\langle 1_L, 1_R \rangle, \langle 2_L, 2_R \rangle)$. We observe that the requirement of planar fat subgraphs, does not split the subgraph into 4 disconnected components, each with two external edges. Instead, as shown in Fig 35, we are left with a subgraph with six external edges. This gives rise to a set of diagrams which, although not melonic, are maximal in the large N limit, such as the one depicted Figure 1.

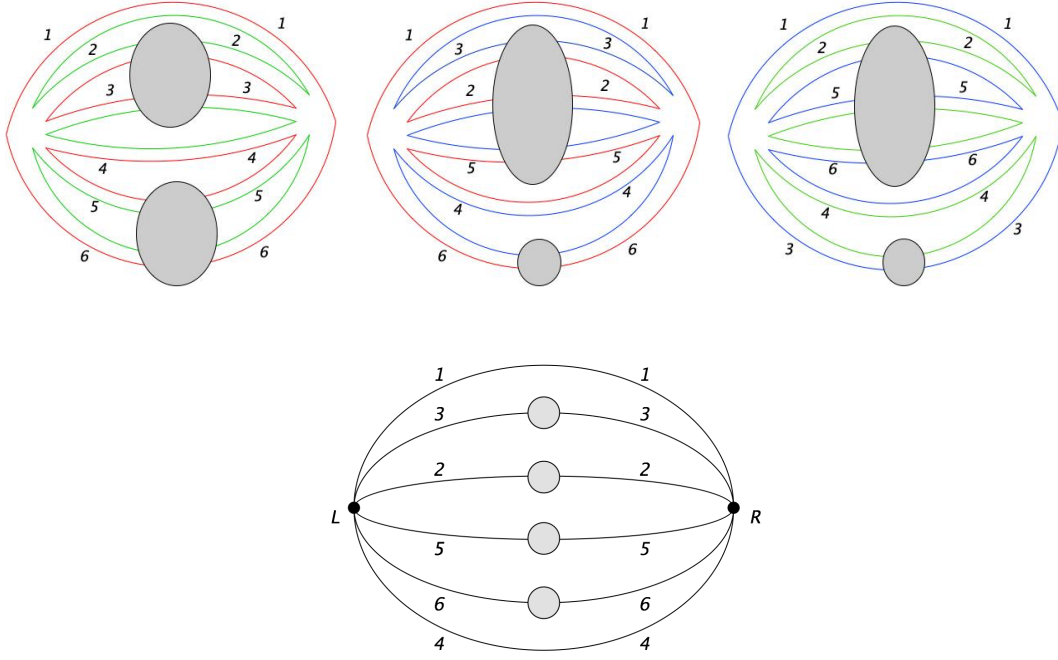


Figure 34: The fat graphs for the loop $(\langle 1_L, 1_R \rangle, \langle 4_L, 4_R \rangle)$ involving two prism interaction vertices are shown above. We see that this gives rise to a conventional melonic structure shown below.

5.3.3 New cutting and sewing argument

In order to obtain a recursive enumeration of diagrams in this case, we need to adapt the cutting and sewing rules given earlier to the subgraph containing 6 external lines. We show how this is done in Figure 36.

The graph on the right in Figure 36 is a free energy graph that contains at least one vertex, so it must take one of the forms enumerated in the previous section. By cutting out one prism interaction vertex from any of these forms, we can determine all the possibilities for subgraph G in Figure 36. We have thus completed our recursive enumeration of all the graphs.

To translate this enumeration into the language of melonic-moves, we note that, in addition to the usual melonic move of replacing a propagator by an elementary snail or melon, Figure 36 requires us to introduce an additional move. In particular, from the possibility that the subgraph G could be obtained from cutting out one interaction vertex from the cycle of Figure 35, we obtain the new “vertex-expansion” move of replacing an interaction vertex by two-interaction vertices contracted in a particular way, as shown in Figure 37.⁷ One can check that under this move, $v \rightarrow v + 1$ and $f_{tot} \rightarrow f_{tot} + r$, so the maximality condition (4.6) is preserved.

⁷We would like to thank Adrian Tanasa and Victor Nador for discussions on this point

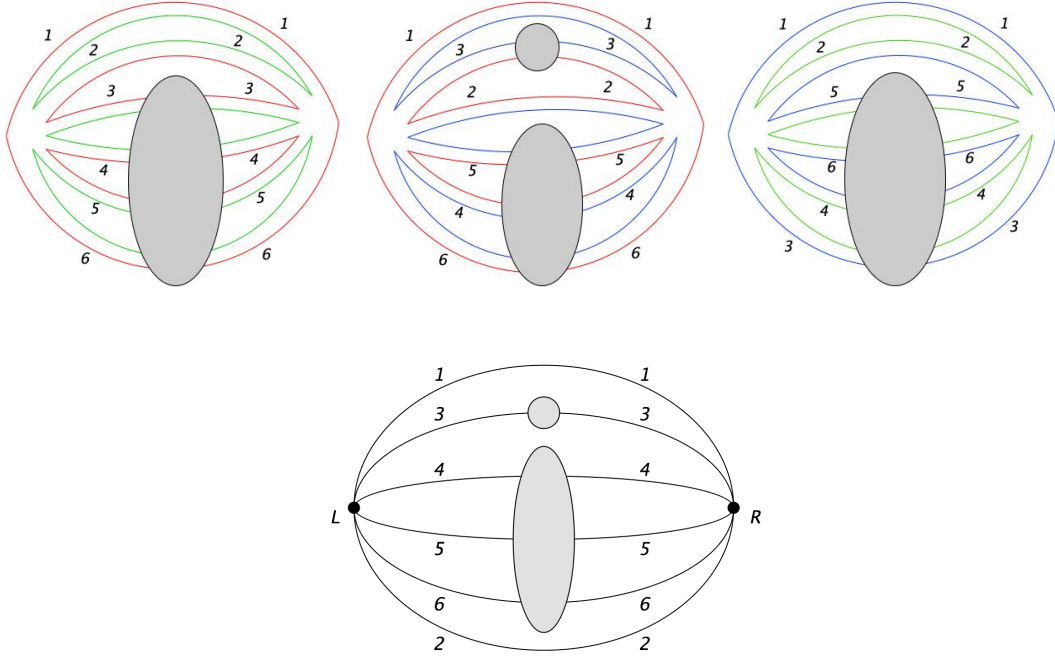


Figure 35: The three fat graphs for the 2-cycle $(\langle 1_L, 1_R \rangle, \langle 2_L, 2_R \rangle)$ involving two prism interaction vertices are shown above. From the blue-red fat-graph, we see that the subgraph gets split into two parts. However, there are not enough constraints to separate the subgraph into 4 components, with two external edges each. Hence the theory is not melonic in a conventional sense.

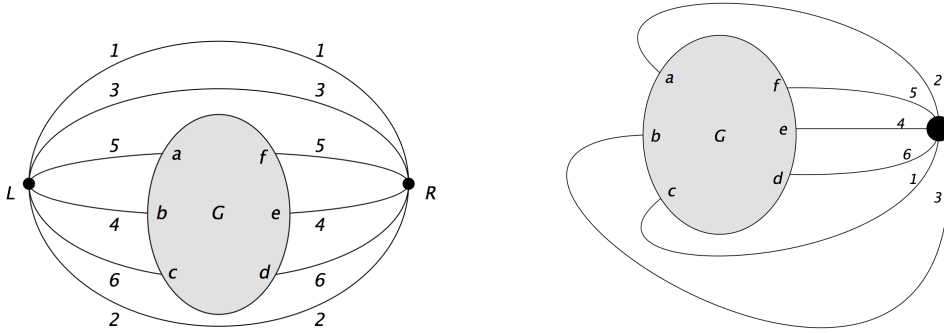


Figure 36: The graph on the left, which originates from the Figure 35, is maximal if and only if the graph on the right is maximal. One can see this by tracing each of the index contractions for each of the three $O(N)$ symmetry groups. The graph on the right is a free energy graph and must be one of the forms enumerated in the previous subsection. The above relation also gives rise to a new elementary move: of replacing one vertex (right) by two vertices (left).

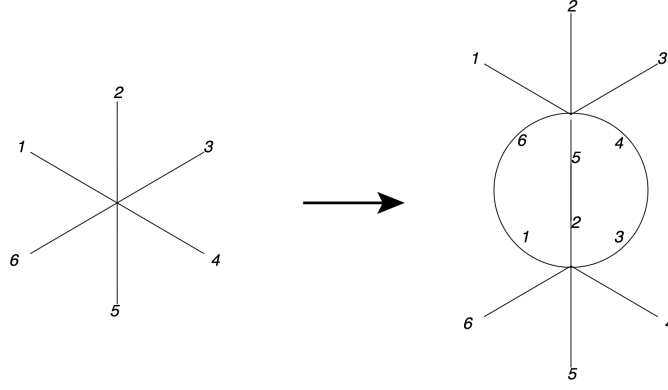


Figure 37: A new melonic move, vertex expansion, is present in the prismatic model.

5.4 Theory with both a prism and wheel

Let us also consider a theory with both $r = 3$ maximally-single-trace interactions, the prism and wheel. The allowed 1-cycles remain those from the prism and wheel theories respectively, but the 2-cycles now also include the possibility of a loop passing through one wheel vertex and one prism vertex. We analyze this case now.

Let us assume the L vertex is a prism and the R vertex is a wheel. As shown in the appendix, the in-equivalent 2-cycles are:

1. $(\langle 1_L, 1_R \rangle, \langle 2_L, W_R \rangle)$,
2. $(\langle 1_L, 1_R \rangle, \langle 4_L, W'_R \rangle)$,
3. $(\langle 1_L, 1_R \rangle, \langle 6_L, 2_R \rangle)$,
4. $(\langle 1_L, 1_R \rangle, \langle 6_L, 3_R \rangle)$,
5. $(\langle 1_L, 1_R \rangle, \langle 6_L, 6_R \rangle)$.

All of the 2-cycles of the form 1, 2 and 4 contain a twist in one of the two-colour fat graphs, and are non-maximal.

Case 3 and Case 5 allow for a double snail. There are no other possibilities. In particular there is no new elementary melon containing both a wheel and a prism vertex, and the elementary moves of the prism theory and the wheel theory generate all Feynman diagrams.

6 Comments on field-theories based on these interactions

In this section we discuss specific realizations of these theories. Let us focus our attention on obtaining IR fixed points with physics similar to the SYK model.

A list of theories involving a single, real rank- r tensor field that can be solved via the analysis given above includes:

1. A quantum-mechanical theory of rank-4 Majorana fermions based on the double-prism interaction.
2. A $d < 3$ dimensional theory of rank-4 real bosons dominated by the double-prism interaction.
3. A $d < 3$ dimensional theory of rank-3 real bosons dominated by the wheel interaction.
4. A $d < 3$ dimensional theory of rank-3 real bosons dominated by the prism interaction.
5. A $d < 3$ dimensional theory of rank-3 real bosons dominated by both the wheel and the prism interaction.

We have argued that $1d$ theory of real, rank-4, fermionic tensors based on the double-prism is dominated by melonic diagrams. Hence we expect its large N saddle point solution will proceed exactly along the lines of [44], and in particular we expect essentially the same spectrum as the $q = 6$ SYK model. It might be interesting to study the theory more carefully, including numerical studies to compare its behaviour at finite N to the rank-5 melonic tensor model studied in [44] or other models [71–76], but we do not do this here.

The bosonic version of this theory, which can be defined for $d < 3$, also dominated by melonic diagrams. Its large N saddle point solution will proceed exactly along the lines of the $q = 6$ bosonic theories discussed in [52]. We illustrate this explicitly in subsection 6.1 below.

For the large N solution of the theory of rank-3 real bosons with a wheel interaction, the only difference from the traditional melonic theory is the presence of the elementary snail. This elementary snail is a tadpole, so it does not appear to affect the results of the Schwinger-Dyson equation for the exact propagator. We, therefore, again expect the large N solution to again proceed along the lines of the $q = 6$ bosonic tensor models discussed in [52]. However, one slightly novel feature of the wheel interaction is that it allows us to define a theory of complex bosons with $U(N)^3$ symmetry group, as its interaction graph is bi-partite.

The large N solution to the theory of rank-3 bosons with a prism interaction was discussed in [43]. We now have the possibility of solving for the large N limit of a theory of rank-3 bosons with both the wheel and prism interactions. We leave this for future work.

6.1 Real sextic bosonic theories with melonic dominance

Let us first consider the rank-4 bosonic theory with double prism interaction. The Lagrangian for this theory is:

$$L = \int d^d x \frac{1}{2} \partial_\mu \phi \partial^\mu \phi + g \phi^{a_1 b_1 c_1 d_1} \phi^{a_1 b_2 c_2 d_2} \phi^{a_2 b_2 c_1 d_3} \phi^{a_2 b_3 c_3 d_1} \phi^{a_3 b_3 c_2 d_3} \phi^{a_3 b_1 c_3 d_2}. \quad (6.1)$$

The 't Hooft coupling for this theory is $\lambda = gN^4$.

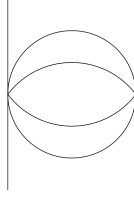


Figure 38: The integration kernel for the four-point function

To write down the gap equation, we need to carefully count all the melonic Wick contractions that take the form of the elementary melon in Figure 31. Let us denote this number by n_{melon} . Here $n_{\text{melon}} = 6$. The gap equation in the strong coupling limit takes the form:

$$G^{-1}(x) = -\lambda^2 n_{\text{melon}} G(x)^6. \quad (6.2)$$

Let us now write the integration kernel:

$$K(x_1, x_2, x_3, x_4) = n_{\text{kernel}} \lambda^2 G(x_{13}) G(x_{24}) G(x_{34})^4, \quad (6.3)$$

where n_{kernel} is the number of melonic Wick contractions of the form given in Figure 38. Clearly, for any melonic Wick contraction that takes the form of the elementary melon, one simply has to choose an internal line to cut, in order to obtain a melonic Wick contraction for the kernel, so $n_{\text{kernel}} = (q - 1)n_{\text{melon}}$, where $q = 6$ in our case. If we now absorb n_{melon} into $\tilde{\lambda}^2 = \lambda^2 n_{\text{melon}}$, our Schwinger-Dyson equations become:

$$G^{-1}(x) = -\tilde{\lambda}^2 G(x)^6. \quad (6.4)$$

and

$$K(x_1, x_2, x_3, x_4) = (q - 1) \tilde{\lambda}^2 G(x_{13}) G(x_{24}) G(x_{34})^4, \quad (6.5)$$

which are identical to those solved in [52].

An identical argument shows that the theory with only a wheel is also given by the solution in [52] for $q = 6$, assuming here that the elementary snail, which is a tadpole, in the gap equation can be made to vanish, say via dimensional regularization.

7 Discussion

In this paper, we classified all real subchromatic sextic tensor models with maximally-single-trace interactions. We showed that, in the natural large N 't Hooft limit, these theories are dominated by melonic (or prismatic) diagrams; and these diagrams can be explicitly enumerated and summed.

We have essentially shown that all rank-3 sextic tensor models are solvable in the large N limit by our analysis of maximal diagrams arising from the wheel interaction. For com-

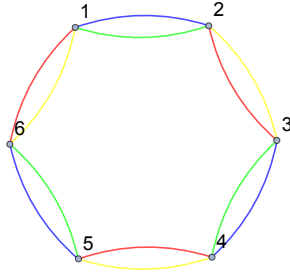


Figure 39: This is a non-MST rank-4 interaction whose large N limit gives rise to all planar diagrams. It is equivalent to the rank-2 MST interaction.

pleteness, we should also explain how to handle the non-MST interactions of [43]. It is easy to see that all the non-MST interactions can be reduced to quartic pillow and double-trace interactions by the introduction of an auxiliary field. Hence, any sextic rank-3 tensor model without a wheel interaction is effectively a quartic-tensor model and is therefore solvable in the large N limit by now-standard techniques. We postpone a detailed study of the most general $r = 3$ sextic theory and its fixed points to future work.

One might ask whether all rank-4 sextic tensor models are solvable. This is apparently not the case – for example, the non-MST interaction shown in Figure 39, is clearly equivalent to a rank-2 MST interaction, and gives rise to all planar diagrams. Such an interaction would exist for any theory based on tensors of even rank.

It would also be straightforward, but potentially very interesting, to extend the analysis of this paper to higher- q ; although, for higher q we are restricted to quantum mechanics models and $d = 2$ bosonic theories.

Acknowledgement

We thank Adrian Tanasa and Victor Nador for discussions. We also thank Igor Klebanov for comments on a draft of this manuscript. RS would like to thank Bordeaux U., LPT, Orsay and IIT, Kanpur for hospitality during the course of this work. RS is partially supported by the Spanish Research Agency (Agencia Estatal de Investigación) through the grants IFT Centro de Excelencia Severo Ochoa SEV-2016-0597, FPA2015-65480-P and PGC2018-095976-B-C21. SP acknowledges the support of a DST INSPIRE faculty award, and DST-SERB grants: MTR/2018/0010077 and ECR/2017/001023.

A Appendix: Finding inequivalent 2-cycles

Here we illustrate a simple method for enumerating inequivalent 2-cycles. We discuss only the case of a 2-cycle passing through two wheel vertices and a 2 cycle passing through a wheel

and a prism vertex. A very similar analysis applies for the other cases.

Wheel

We represent the symmetry group as a group of permutations acting on the twelve labelled field-vertices $\{1_L, 2_L, \dots, 6_L, 1_R, 2_R, \dots, 6_R\}$. Colour permutations simultaneously act on both vertices, while automorphisms can act on each vertex independently. Hence the colour permutation generators act as

$$\sigma_{rg} = (1_L, 5_L)(2_L, 4_L)(1_R, 5_R)(2_R, 4_R), \quad (\text{A.1})$$

and

$$\sigma_{gb} = (1_L, 5_L)(4_L, 6_L)(1_R, 5_R)(4_R, 6_R). \quad (\text{A.2})$$

The automorphisms are generated by the permutations

$$(1_L, 6_L)(2_L, 5_L)(3_L, 4_L),$$

$$(1_L, 2_L)(4_L, 5_L)(3_L, 6_L),$$

$$(1_R, 6_R)(2_R, 5_R)(3_R, 4_R)$$

and

$$(1_R, 2_R)(4_R, 5_R)(3_R, 6_R).$$

The total symmetry group of colour permutations and automorphisms, which we are representing as a subgroup of S_{12} , has 216 elements.

For determining the inequivalent choices for X_L , we first note that the orbit of 1_L is $\{1_L, 2_L, 3_L, 4_L, 5_L, 6_L\}$. Hence, any choice of X_L can be related to $X_L = 1_L$ without loss of generality.

We are then left with a residual symmetry group: the stabilizer of 1_L , which contains 36 elements. We then find the orbit of 1_R in this residual symmetry group is $\{1_R, 2_R, 3_R, 4_R, 5_R, 6_R\}$. Hence we can take $Y_R = 1_R$. We next consider the residual symmetry group that stabilizes both 1_L and 1_R , which contains 6 elements. We find its orbits include $\{2_L, 4_L, 6_L\}$ and $\{3_L, 5_L\}$. Hence we can take $Z_L = 2_L$ or 3_L .

The inequivalent 2-cycles so far are thus:

1. $(\langle 1_L, 1_R \rangle, \langle 2_L, W_R \rangle)$,
2. $(\langle 1_L, 1_R \rangle, \langle 3_L, W'_R \rangle)$.

We now consider the residual symmetry group that stabilizes 1_L , 1_R , and 2_L , which contains two elements. The orbits of this symmetry group are $\{2_R\}$, $\{3_R, 5_R\}$, and $\{4_R, 6_R\}$. Hence the inequivalent choices for W_R are 2_R , 3_R and 4_R . We also consider the residual

symmetry group that stabilizes 1_L , 1_R , and 3_L , which contains 3 elements. Its orbits are: $\{3_R\}$, $\{5_R\}$, and $\{2_R, 4_R, 6_R\}$. The inequivalent choices for W'_R are thus $2_R, 3_R$ and 5_R .

Prism and wheel

Let us consider a 2-cycle which intersects one prism interaction vertex and one wheel interaction vertex. Let us assume the left (L) vertex is a prism and the right (R) vertex is a wheel.

The combined colour permutation and automorphism symmetry group contains 72 elements. The orbit of 1_L under this group is $\{1_L, \dots, 6_L\}$, so we can take $X_L = 1_L$.

The residual symmetry group that stabilizes 1_L has 12 elements. The orbit of 1_R under this residual symmetry group is $\{1_R, \dots, 6_R\}$, so we can choose $Y_R = 1_R$.

The residual symmetry group that stabilizes both 1_L and 1_R has 2 elements. Its orbits include $\{2_L, 3_L\}$ and $\{4_L, 5_L\}$. Hence we can take $Z_L = 2_L, 4_L$, or 6_L . If we choose $Z_L = 6_L$, then there is still a residual symmetry group and we can take $W_R = 2_R, 3_R$ or 6_R .

The inequivalent 2-cycles are thus:

1. $(\langle 1_L, 1_R \rangle, \langle 2_L, W_R \rangle)$,
2. $(\langle 1_L, 1_R \rangle, \langle 4_L, W'_R \rangle)$,
3. $(\langle 1_L, 1_R \rangle, \langle 6_L, 2_R \rangle)$,
4. $(\langle 1_L, 1_R \rangle, \langle 6_L, 3_R \rangle)$,
5. $(\langle 1_L, 1_R \rangle, \langle 6_L, 6_R \rangle)$.

References

- [1] G. 't Hooft, “A Planar Diagram Theory for Strong Interactions,” *Nucl.Phys.* **B72** (1974) 461.
- [2] M. Moshe and J. Zinn-Justin, “Quantum field theory in the large N limit: A Review,” *Phys. Rept.* **385** (2003) 69–228, [hep-th/0306133](#).
- [3] R. Gurau, “Colored Group Field Theory,” *Commun. Math. Phys.* **304** (2011) 69–93, [0907.2582](#).
- [4] R. Gurau and V. Rivasseau, “The $1/N$ expansion of colored tensor models in arbitrary dimension,” *Europhys. Lett.* **95** (2011) 50004, [1101.4182](#).
- [5] R. Gurau, “The complete $1/N$ expansion of colored tensor models in arbitrary dimension,” *Annales Henri Poincaré* **13** (2012) 399–423, [1102.5759](#).
- [6] V. Bonzom, R. Gurau, A. Riello, and V. Rivasseau, “Critical behavior of colored tensor models in the large N limit,” *Nucl. Phys.* **B853** (2011) 174–195, [1105.3122](#).

- [7] A. Tanasa, “Multi-orientable Group Field Theory,” *J. Phys.* **A45** (2012) 165401, 1109.0694.
- [8] V. Bonzom, R. Gurau, and V. Rivasseau, “Random tensor models in the large N limit: Uncoloring the colored tensor models,” *Phys. Rev.* **D85** (2012) 084037, 1202.3637.
- [9] S. Carrozza and A. Tanasa, “ $O(N)$ Random Tensor Models,” *Lett. Math. Phys.* **106** (2016), no. 11 1531–1559, 1512.06718.
- [10] E. Witten, “An SYK-Like Model Without Disorder,” 1610.09758.
- [11] I. R. Klebanov and G. Tarnopolsky, “Uncolored random tensors, melon diagrams, and the Sachdev-Ye-Kitaev models,” *Phys. Rev.* **D95** (2017), no. 4 046004, 1611.08915.
- [12] R. Gurau, “Invitation to Random Tensors,” *SIGMA* **12** (2016) 094, 1609.06439.
- [13] N. Delporte and V. Rivasseau, “The Tensor Track V: Holographic Tensors,” 2018. 1804.11101.
- [14] I. R. Klebanov, F. Popov, and G. Tarnopolsky, “TASI Lectures on Large N Tensor Models,” *PoS TASI2017* (2018) 004, 1808.09434.
- [15] R. Gurau, “Notes on Tensor Models and Tensor Field Theories,” 1907.03531.
- [16] S. Sachdev and J. Ye, “Gapless spin fluid ground state in a random, quantum Heisenberg magnet,” *Phys. Rev. Lett.* **70** (1993) 3339, cond-mat/9212030.
- [17] A. Kitaev, “A simple model of quantum holography,” <http://online.kitp.ucsb.edu/online/entangled15/kitaev/>, <http://online.kitp.ucsb.edu/online/entangled15/kitaev2/> Talks at KITP, April 7 and May 27, 2015.
- [18] J. Maldacena and D. Stanford, “Remarks on the Sachdev-Ye-Kitaev model,” *Phys. Rev.* **D94** (2016), no. 10 106002, 1604.07818.
- [19] J. Polchinski and V. Rosenhaus, “The Spectrum in the Sachdev-Ye-Kitaev Model,” *JHEP* **04** (2016) 001, 1601.06768.
- [20] J. Maldacena, D. Stanford, and Z. Yang, “Conformal symmetry and its breaking in two dimensional Nearly Anti-de-Sitter space,” *PTEP* **2016** (2016), no. 12 12C104, 1606.01857.
- [21] J. Engelsöy, T. G. Mertens, and H. Verlinde, “An investigation of AdS_2 backreaction and holography,” *JHEP* **07** (2016) 139, 1606.03438.
- [22] K. Jensen, “Chaos in AdS_2 Holography,” *Phys. Rev. Lett.* **117** (2016), no. 11 111601, 1605.06098.
- [23] A. Jevicki, K. Suzuki, and J. Yoon, “Bi-Local Holography in the SYK Model,” *JHEP* **07** (2016) 007, 1603.06246.
- [24] A. M. Garcia-Garcia and J. J. M. Verbaarschot, “Spectral and thermodynamic properties of the Sachdev-Ye-Kitaev model,” *Phys. Rev.* **D94** (2016), no. 12 126010, 1610.03816.

- [25] J. S. Cotler, G. Gur-Ari, M. Hanada, J. Polchinski, P. Saad, S. H. Shenker, D. Stanford, A. Streicher, and M. Tezuka, “Black Holes and Random Matrices,” *JHEP* **05** (2017) 118, 1611.04650.
- [26] T. Nishinaka and S. Terashima, “A Note on Sachdev-Ye-Kitaev Like Model without Random Coupling,” 1611.10290.
- [27] P. Narayan and J. Yoon, “SYK-like Tensor Models on the Lattice,” 1705.01554.
- [28] A. M. Garcia-Garcia and J. J. M. Verbaarschot, “Analytical Spectral Density of the Sachdev-Ye-Kitaev Model at finite N ,” *Phys. Rev.* **D96** (2017), no. 6 066012, 1701.06593.
- [29] D. J. Gross and V. Rosenhaus, “The Bulk Dual of SYK: Cubic Couplings,” *JHEP* **05** (2017) 092, 1702.08016.
- [30] S. R. Das, A. Jevicki, and K. Suzuki, “Three Dimensional View of the SYK/AdS Duality,” *JHEP* **09** (2017) 017, 1704.07208.
- [31] S. R. Das, A. Ghosh, A. Jevicki, and K. Suzuki, “Space-Time in the SYK Model,” *JHEP* **07** (2018) 184, 1712.02725.
- [32] S. R. Das, A. Ghosh, A. Jevicki, and K. Suzuki, “Three Dimensional View of Arbitrary q SYK models,” *JHEP* **02** (2018) 162, 1711.09839.
- [33] G. Mandal, P. Nayak, and S. R. Wadia, “Coadjoint orbit action of Virasoro group and two-dimensional quantum gravity dual to SYK/tensor models,” 1702.04266.
- [34] P. Gao, D. L. Jafferis, and A. Wall, “Traversable Wormholes via a Double Trace Deformation,” *JHEP* **12** (2017) 151, 1608.05687.
- [35] J. Maldacena, D. Stanford, and Z. Yang, “Diving into traversable wormholes,” *Fortsch. Phys.* **65** (2017), no. 5 1700034, 1704.05333.
- [36] J. Maldacena and X.-L. Qi, “Eternal traversable wormhole,” 1804.00491.
- [37] J. Kim, I. R. Klebanov, G. Tarnopolsky, and W. Zhao, “Symmetry Breaking in Coupled SYK or Tensor Models,” *Phys. Rev.* **X9** (2019), no. 2 021043, 1902.02287.
- [38] V. Rosenhaus, “An introduction to the SYK model,” *J. Phys.* **A52** (2019), no. 32 323001.
- [39] S. Choudhury, A. Dey, I. Halder, L. Janagal, S. Minwalla, and R. Poojary, “Notes on Melonic $O(N)^{q-1}$ Tensor Models,” 1707.09352.
- [40] K. Bulycheva, I. R. Klebanov, A. Milekhin, and G. Tarnopolsky, “Spectra of Operators in Large N Tensor Models,” 1707.09347.
- [41] F. Ferrari, V. Rivasseau, and G. Valette, “A New Large N Expansion for General Matrix-Tensor Models,” 1709.07366.
- [42] S. S. Gubser, C. Jepsen, Z. Ji, and B. Trundy, “Higher melonic theories,” *JHEP* **09** (2018) 049, 1806.04800.
- [43] S. Giombi, I. R. Klebanov, F. Popov, S. Prakash, and G. Tarnopolsky, “Prismatic Large N Models for Bosonic Tensors,” *Phys. Rev.* **D98** (2018), no. 10 105005, 1808.04344.

- [44] I. R. Klebanov, P. N. Pallegar, and F. K. Popov, “Majorana Fermion Quantum Mechanics for Higher Rank Tensors,” 1905.06264.
- [45] O. Aharony, O. Bergman, D. L. Jafferis, and J. Maldacena, “N=6 superconformal Chern-Simons-matter theories, M2-branes and their gravity duals,” *JHEP* **0810** (2008) 091, 0806.1218.
- [46] V. Gurucharan and S. Prakash, “Anomalous dimensions in non-supersymmetric bifundamental Chern-Simons theories,” *JHEP* **09** (2014) 009, 1404.7849. [Erratum: *JHEP*11,045(2017)].
- [47] J. Murugan, D. Stanford, and E. Witten, “More on Supersymmetric and 2d Analogs of the SYK Model,” 1706.05362.
- [48] L. Lionni and J. Thürigen, “Multi-critical behaviour of 4-dimensional tensor models up to order 6,” *Nucl. Phys.* **B941** (2019) 600–635, 1707.08931.
- [49] V. Bonzom, L. Lionni, and V. Rivasseau, “Colored triangulations of arbitrary dimensions are stuffed Walsh maps,” *arXiv preprint arXiv:1508.03805* (2015).
- [50] I. R. Klebanov and G. Tarnopolsky, “On Large N Limit of Symmetric Traceless Tensor Models,” *JHEP* **10** (2017) 037, 1706.00839.
- [51] D. Benedetti, S. Carrozza, R. Gurau, and M. Kolanowski, “The $1/N$ expansion of the symmetric traceless and the antisymmetric tensor models in rank three,” 1712.00249.
- [52] S. Giombi, I. R. Klebanov, and G. Tarnopolsky, “Bosonic Tensor Models at Large N and Small ϵ ,” 1707.03866.
- [53] S. Prakash and R. Sinha, “A Complex Fermionic Tensor Model in d Dimensions,” *JHEP* **02** (2018) 086, 1710.09357.
- [54] J. Ben Geloun and V. Rivasseau, “A Renormalizable SYK-type Tensor Field Theory,” *Annales Henri Poincaré* **19** (2018), no. 11 3357–3395, 1711.05967.
- [55] D. Benedetti, S. Carrozza, R. Gurau, and A. Sfondrini, “Tensorial Gross-Neveu models,” *JHEP* **01** (2018) 003, 1710.10253.
- [56] C. Peng, M. Spradlin, and A. Volovich, “A Supersymmetric SYK-like Tensor Model,” *JHEP* **05** (2017) 062, 1612.03851.
- [57] C. Peng, M. Spradlin, and A. Volovich, “Correlators in the $\mathcal{N} = 2$ Supersymmetric SYK Model,” *JHEP* **10** (2017) 202, 1706.06078.
- [58] A. Mironov and A. Morozov, “Correlators in tensor models from character calculus,” *Phys. Lett.* **B774** (2017) 210–216, 1706.03667.
- [59] H. Itoyama, A. Mironov, and A. Morozov, “Ward identities and combinatorics of rainbow tensor models,” *JHEP* **06** (2017) 115, 1704.08648.
- [60] H. Itoyama, A. Mironov, and A. Morozov, “Cut and join operator ring in tensor models,” *Nucl. Phys.* **B932** (2018) 52–118, 1710.10027.
- [61] D. Benedetti and N. Delporte, “Phase diagram and fixed points of tensorial Gross-Neveu models in three dimensions,” *JHEP* **01** (2019) 218, 1810.04583.

- [62] D. Benedetti and R. Gurau, “2PI effective action for the SYK model and tensor field theories,” *JHEP* **05** (2018) 156, 1802.05500.
- [63] C.-M. Chang, S. Colin-Ellerin, and M. Rangamani, “On Melonic Supertensor Models,” *JHEP* **10** (2018) 157, 1806.09903.
- [64] D. Benedetti, R. Gurau, and S. Harribey, “Line of fixed points in a bosonic tensor model,” *JHEP* **06** (2019) 053, 1903.03578.
- [65] C.-M. Chang, S. Colin-Ellerin, and M. Rangamani, “Supersymmetric Landau-Ginzburg Tensor Models,” 1906.02163.
- [66] F. K. Popov, “Supersymmetric Tensor Model at Large N and Small ϵ ,” 1907.02440.
- [67] F. Ferrari and F. I. Schaposnik Massolo, “Phases Of Melonic Quantum Mechanics,” *Phys. Rev.* **D100** (2019), no. 2 026007, 1903.06633.
- [68] H. Osborn and A. Stergiou, “Seeking fixed points in multiple coupling scalar theories in the ϵ expansion,” *JHEP* **05** (2018) 051, 1707.06165.
- [69] V. Bonzom, V. Nador, and A. Tanasa, “Diagrammatic proof of the large N melonic dominance in the SYK model,” 1808.10314.
- [70] S. Giombi, S. Minwalla, S. Prakash, S. P. Trivedi, S. R. Wadia, *et. al.*, “Chern-Simons Theory with Vector Fermion Matter,” *Eur.Phys.J.* **C72** (2012) 2112, 1110.4386.
- [71] C. Krishnan, K. V. P. Kumar, and S. Sanyal, “Random Matrices and Holographic Tensor Models,” *JHEP* **06** (2017) 036, 1703.08155.
- [72] C. Krishnan and K. V. P. Kumar, “Towards a Finite- N Hologram,” *JHEP* **10** (2017) 099, 1706.05364.
- [73] C. Krishnan and K. V. Pavan Kumar, “Exact Solution of a Strongly Coupled Gauge Theory in 0+1 Dimensions,” *Phys. Rev. Lett.* **120** (2018), no. 20 201603, 1802.02502.
- [74] I. R. Klebanov, A. Milekhin, F. Popov, and G. Tarnopolsky, “Spectra of eigenstates in fermionic tensor quantum mechanics,” *Phys. Rev.* **D97** (2018), no. 10 106023, 1802.10263.
- [75] C. Krishnan and K. V. Pavan Kumar, “Complete Solution of a Gauged Tensor Model,” 1804.10103.
- [76] K. Pakrouski, I. R. Klebanov, F. Popov, and G. Tarnopolsky, “Spectrum of Majorana Quantum Mechanics with $O(4)^3$ Symmetry,” *Phys. Rev. Lett.* **122** (2019), no. 1 011601, 1808.07455.